Gulf Stream path and thermocline structure near 74°W and 68°W

D. Randolph Watts and Karen L. Tracey

Graduate School of Oceanography, University of Rhode Island, Narragansett

John M. Bane and Thomas J. Shay

Marine Sciences Program, University of North Carolina, Chapel Hill

Abstract. The SYNoptic Ocean Prediction (SYNOP) experiment had the goal of providing a physical understanding of energetic mesoscale eddy processes in the Gulf Stream. In the SYNOP Inlet Array off Cape Hatteras and in the Central Array near 68°W moored observations were collected from October 1987 through August 1990. The Inlet Array measured the surface path and bottom currents where the Gulf Stream leaves the continental margin to enter the deep water regime; small amplitude propagating and growing meanders characterized the variability there. The Central Array measured velocity and temperature (as a proxy for density) at four levels in the water column, as well as the upper and deep level streamfunctions, all with mesoscale resolution. Near 70°W the path envelope exhibited a relative node, confined within a 40-km band 55% of the time. Near 68°W the path envelope was over 3 times as wide, due to several elongated ("steep") meander troughs and relatively steep meander crests. The crests typically propagated downstream without much growth. The troughs often stalled near 68°W, steepened, and persisted for one to several months. Two cases evolved into "S-shaped" paths and subsequently formed rings. Even the time-averaged fields showed a small trough in the mean path and thermocline structure. Whereas meanders of 20- to 60-day periods had similar spectral levels throughout 70°–67°W, meanders with long periods (> 85 day) accounted for the local minimum in variance at 70°W. Bottom pressure and velocity observations revealed repeated periods of intense (swirl speeds > 0.30 m s^{-1}) abyssal eddies; the time-averaged deep currents exhibited a mean cyclone centered 30 km offshore and downstream of the upper layer mean trough. The cross-stream slope of the thermocline steepened linearly with path curvature, consistent with gradient wind balance. Structures are illustrated in the mapped fields consistent with baroclinic instability wherein troughs steepen and rings form.

Introduction

Mesoscale variability is intrinsic to the Gulf Stream system, evident in meandering of the baroclinic density front and current, and in the formation of cutoff rings. These phenomena have been observed in various levels of detail for several decades, as described in overview articles by *Fofonoff* [1981], *Watts* [1983], and *Richardson* [1983]. Interactions between the Gulf Stream and its surrounding rings and eddies exchange momentum, energy, and vorticity. Such exchanges and their associated modifications are present both in observations [*Cronin*, 1993]; and in numerical models of the Gulf Stream [*Robinson et al.*, 1988]. Similar processes are observed in the atmospheric jet stream [*Palmén and Newton*, 1969].

Studying the Gulf Stream has long been challenging, both technologically and dynamically, for physical oceanographers because of the broad range of temporal and spatial

scales involved. The goal of the combined SYNOP (SYNoptic Ocean Prediction) observational, theoretical, and modeling studies was to achieve a dynamically accurate understanding of the Gulf Stream and its energetic mesoscale meandering processes. Figure 1 summarizes the SYNOP moored array program.

This paper is Part 1 of two articles that focus upon the moored instrument studies conducted in the SYNOP "Central Array," near 68°W. Results from the small "Inlet Array," near 74°W, off Cape Hatteras are also reported herein. These articles present an overview of the experimental design and data set as a whole, and they will provide a summary reference for other articles and works in progress.

The subsequent sections have the following goals: (1) Present the basic statistics on the path, thermocline structure, and abyssal streamfunction; (2) Summarize their variance and spectral properties, to serve as benchmarks against which models should be tested; (3) Illustrate representative processes, utilizing the ability from these moored observations to map the dynamical fields in four dimensions (x, y, z, t) with mesoscale resolution.

T. J. Shay et al. (Gulf Stream flow field and events at 68°W, submitted to *Journal of Geophysical Research*,

SYNOP Moored Array Program
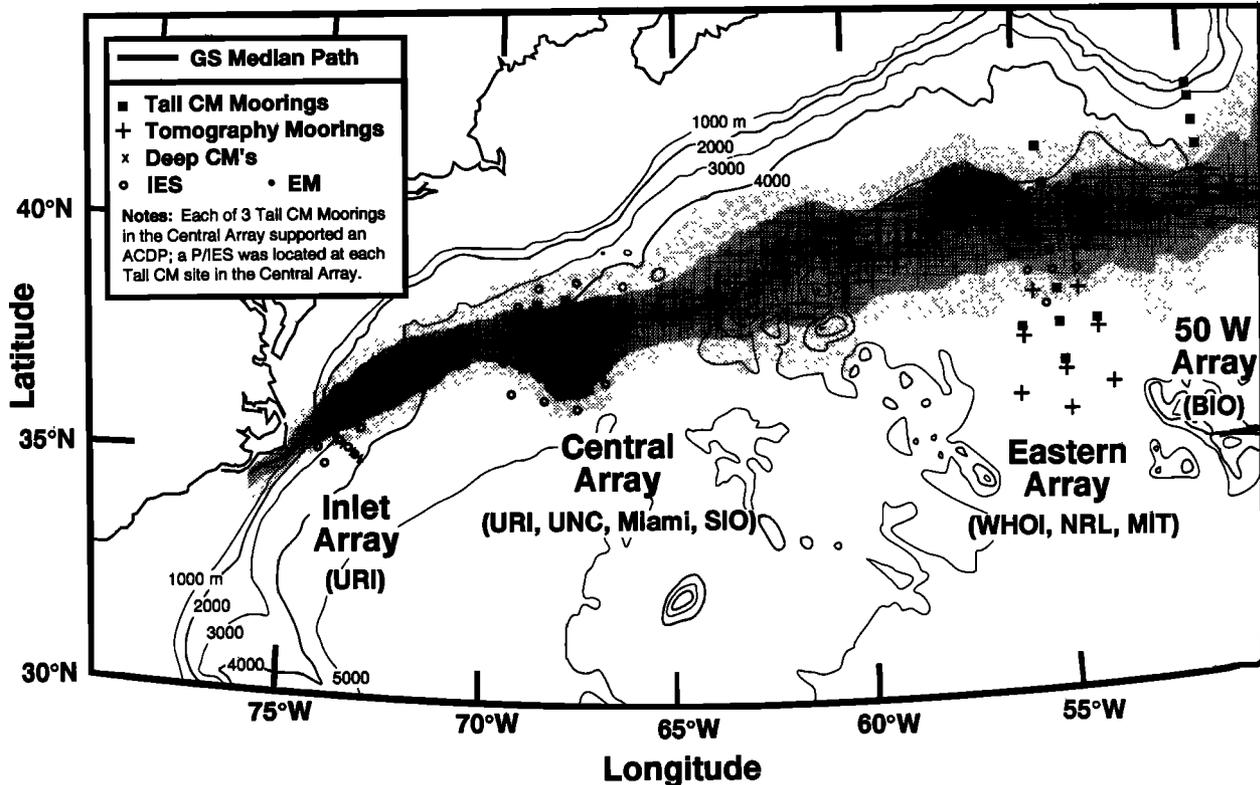
Figure 1. SYNOP moored array program during 1987–1990. Current meter moorings (crosses and solid squares) and inverted echo sounders (open circles) were concentrated in three regions: the Inlet, Central and Eastern Arrays. Four horizontal electric field (EM) meters (solid dots) were deployed in the Central Array and eight tomography moorings were deployed in the Eastern Array. Additionally, current meter moorings were maintained along a meridonal section at 50°W. The northern edge of the Gulf Stream derived from satellite imagery is indicated by the track of median positions (dark line) and the 10–90% and 1–99% probability ranges (dark and light shading, respectively) for the period May 1988 through August 1990.

1995, hereinafter referred to as Part 2) present the structure of the flow field observed in geographic coordinates and its corresponding statistics, and illustrates the temporal development of selected processes. A related article by *Johns et al.* [1995] presents the synoptic Gulf Stream, that is, the velocity structure and transport averaged in stream-coordinates, revealing features in the current and in the adjacent recirculation fields that are otherwise hidden by geographic averages.

Observations

Figure 1 shows the full SYNOP moored array program, including the Inlet and Central Arrays and two arrays located farther to the east. The array near 55°W has been reported in *Hogg* [1993] and A. S. Bower and N. G. Hogg (On the structure of the Gulf Stream and its recirculations at 55°W, submitted to *Journal of Physical Oceanography*, 1995). Figure 1 also shows the track of median positions and envelope of meandering of the north edge of the Gulf Stream, determined for the same time period that our SYNOP moorings were deployed.

A short general description of the moored arrays is given in Part 1 and Part 2 so that each paper may be read on its own. Details about the inverted echo sounder (IES) and pressure instrumentation, measurements, and data-processing techniques appear in Part 1, because its focus is upon the path, thermocline structure, and bottom pressure fields. Details about the current meter records appear in Part 2, because its focus is upon the structure and evolution of the flow field. Part 1 summarizes objective mapping for all the fields.

Moored Arrays

The array sites shown in Figure 2 were maintained for 26 months, (October 1987 to September 1990). The bathymetry from Cape Hatteras to the New England Seamounts is also indicated.

The Inlet Array crossed the continental slope northeast of Cape Hatteras. Its purpose was to monitor "inflow conditions," such as the upper level path and deep currents, as the Gulf Stream leaves the continental margin. Hence the Inlet Array data may be assimilated as the upstream boundary conditions for Gulf Stream models by other investigators.
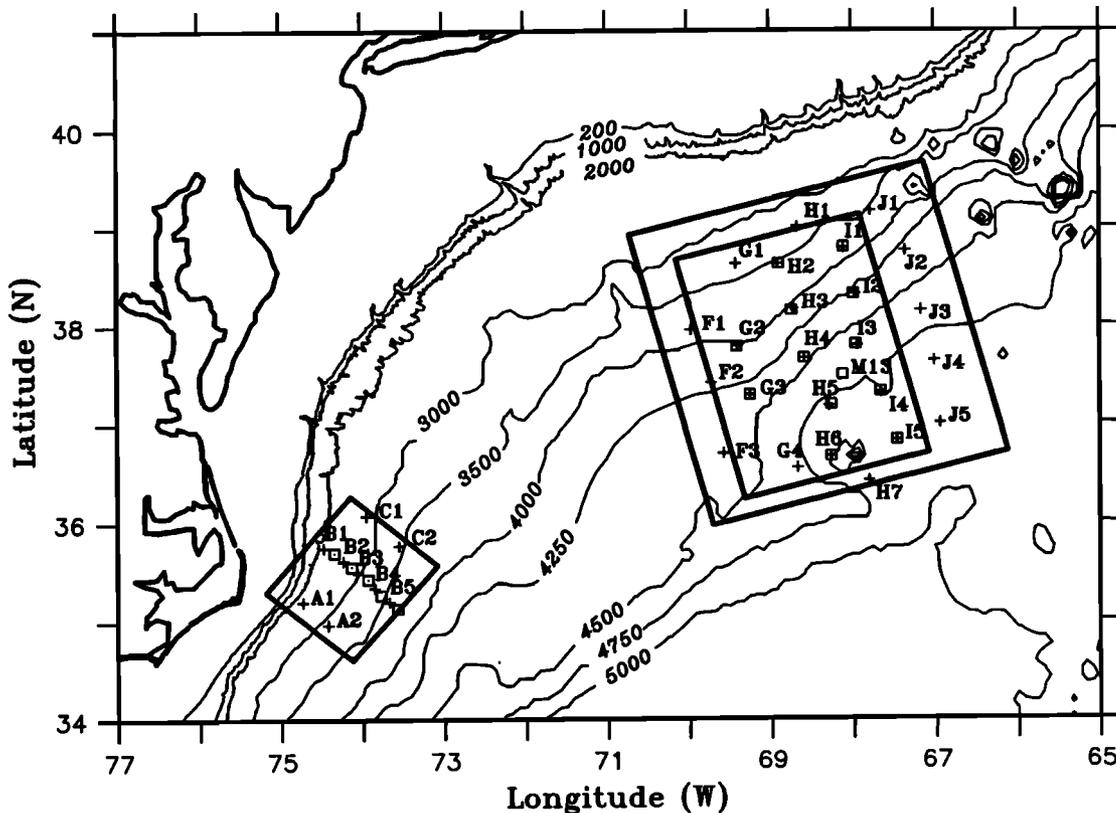
Figure 2. Enlargement of the Inlet and Central Arrays. Current meter moorings are denoted by the open squares and inverted echo sounder sites by the plus symbols. The boxes indicate the regions that have been mapped by optimal interpolation. The box at the Inlet Array and the larger box at the Central Array indicate Z_{12}^* mapping regions; the smaller box at the Central Array indicates the T, ψ, and P_{3500} mapping regions. Bathymetric contours are in meters.

The Inlet Array comprised nine IESs distributed on three lines across the Gulf Stream. The downstream spacing between the three lines was approximately 40 km and the cross-stream spacing was 25 km along the central line (line B) and about 50 km on lines A and C. In addition, five deep current meters were moored at the midpoints between the IESs on line B. Those current meters were positioned 100 m off the bottom so that they would remain out of the bottom boundary layer. This configuration remained for 34 months (October 1987 to September 1990); however, during mid-June 1988 through August 1989 both IESs on line A failed, resulting in Gulf Stream path observations along only two of the three lines. *Pickart and Watts* [1990] and *Pickart* [1994 and 1995] report on these measurements and the relationship to topographic Rossby waves (TRWs) and the Deep Western Boundary Current (DWBC).

The Central Array was centered at 37.5°N and 67.5°W. Its purpose was to map the spatial and temporal structures of the dynamical fields synoptically and at mesoscale resolution. In horizontal dimensions, this set of moored instrumentation spanned meridionally the envelope of Gulf Stream meandering and the area of ring/stream interactions, and it extended downstream through about a typical meander wavelength. The eddy correlation lengths were known ahead of time and were used to guide the experimental design. The instrument spacings were chosen

as a compromise between (1) obtaining correlated records for mapping the energetic mesoscale fluctuations, with sufficient horizontal resolution to determine the dynamically important field gradients, and (2) incorporating a degree of measurement redundancy so that mapped results would be robust to loss of data at isolated measurement sites, versus (3) extending the array to obtain simultaneous coverage across a larger region.

The Central Array had two different configurations. In the "startup" configuration, between October 1987 and June 1988, the Central Array comprised 15 IESs distributed over three cross-stream lines (approximately the same locations as lines G, H, and I in Figure 2). Those instruments were spaced approximately 75 km in both cross-stream and alongstream directions. In the second configuration, from June 1988 through August 1990, 24 IESs were redeployed in the arrangement shown in Figure 2, comprising five lines separated downstream by 60–70 km. The nominal cross-stream spacing was 55 km in the central portion of the array and nearly 70 km at the periphery. (Some of the site locations were shifted a few kilometers to intersect Geosat suborbital tracks in order to facilitate comparisons with sea surface height measurements from the Geosat altimeter [*Kelly and Watts*, 1994].)

The second configuration also included 12 tall current meter moorings (Figure 2). Each mooring had four cur-

rent meters, located at water depths of 400, 700, 1000, and 3500 m. The 12 IESs located near the bases of the current moorings included pressure gauges. Three of the moorings (sites H3, H4, and I2 in Figure 2) had upward-looking acoustic doppler current profilers (ADCP) with temperature and pressure sensors mounted 12 m above the top current meter. These measured the velocities throughout the upper 400 m of the water column. In the summer of 1989, when eight of the moorings were recovered and redeployed, a thirteenth mooring was deployed for the final 1-year period. The final recovery of all the instruments occurred during August–September 1990.

Data Processing

During the SYNOP field program, the sampling intervals of the IESs and current meters ranged from 15 to 60 min depending on the type of instrumentation, length of deployment, and available instrument memory. The current meter velocity and temperature records were compensated for vertical excursions taken by the stiff, but tall, moorings according to a procedure documented in *Cronin et al.* [1992b] and reviewed in Part 2.

Subsequently, all records were treated consistently regardless of data type. In order to remove the subinertial and tidal fluctuations, the records were low-pass filtered using a second-order Butterworth filter with a cutoff period of 40 hours. The filter passed forward and backward in time, to avoid introducing phase shifts. Twenty hours of data at each end of the filtered series were discarded to avoid startup transients. After filtering, all time series were subsampled at 6-hour intervals centered at 0000, 0600, 1200, and 1800 UT.

Processing of the IES travel time and pressure (P_{3500}) data is documented in technical reports [*Qian et al.*, 1990; *Fields and Watts*, 1990, 1991]. The IES travel time observations are converted into measurements of Z_{12}^*, the depth of the thermocline as indicated by the 12°C isotherm, with an accuracy of 19 m [*Howden et al.*, 1993]. The overall data return rates for the Inlet or Central Arrays were 93% for Z_{12}^* and 94% for P_{3500}.

Processing of the current meter data is documented in *Pickart et al.* [1991] for the Inlet Array and in *Shay et al.* [1994] for the Central Array. These technical reports discuss the accuracy of the temperature, velocity, and pressure data, as reviewed in Part 2. *Johns and Zantopp* [1991] documents the processing and accuracy of the ADCP measurements.

The diversity and redundancy of the data set could be exploited to fill some of the data gaps. At mooring sites where IESs were absent, the current meter temperature records at 400, 700, and 1000 m were utilized to generate Z_{12}^* estimates and incorporated into the objective maps of the thermocline depth field. Conversely, at IES sites where moorings were absent, such as on the periphery of the array, the IES Z_{12}^* time series were used to estimate temperature records at desired levels [*Cronin et al.*, 1992b] to improve the spatial extent and quality of the mapped temperature fields. This technique and the accuracies of the simulated records are discussed by *Cronin* [1993].

Objective Mapping

The Z_{12}^*, temperature, current velocity, and pressure data were each mapped onto 20-km (x, y) grids at their respective depth levels using optimal interpolation (OI) following the Gauss-Markov methods of *Bretherton et al.* [1976]. For each input and output variable the empirically fitted correlation functions and the specification of measurement noise level are key factors in the OI procedure. In particular, the current velocities were mapped assuming a horizontally nondivergent correlation function for their streamfunction ψ. Complete details of the OI control factors are reported respectively as follows: for Z_{12}^* mapping, see *Tracey and Watts* [1991a, b] and *Howden et al.* [1993]; for T, (u, v), and ψ mapping, see *Cronin* [1993].

A new capability is employed to map the deep velocity and dynamic pressure field, at 3500 m [*Qian and Watts*, 1992]. It is highlighted here because the combination of deep pressure maps with thermocline depth maps is so useful to elucidate the coupling between the near surface jet and the deep layer. The OI maps of pressure referenced to 3500 m (P_{3500}) utilize both the bottom pressure gauge and the deep current meter velocity measurements, using correlation functions that assume geostrophy at this deep level. A reference pressure is determined for each bottom pressure record to be consistent with the mean geostrophic streamfunction field mapped from the deep current meters. The benefit is that all P_{3500} maps have a spatially consistent reference level between sites and a time-independent reference level for all the daily maps.

Altogether, OI maps were created for current streamfunction and temperature (ψ, T) at four depth horizons (400, 700, 1000, and 3500 m) and for thermocline depth Z_{12}^* and pressure P_{3500}. The maps are centered at 1200 UT each day throughout the SYNOP time period. The boxes in Figure 2 indicate the mapping regions. For the Central Array, the Z_{12}^* region extended 320 km downstream by 340 km cross stream with its bottom edge oriented along 075°T. The maps of ψ, T and P_{3500} covered a smaller region (200 km by 280 km) due to the more limited extent of current mooring and pressure sites. The mapping region for Z_{12}^* in the Inlet Array was 140 km by 120 km, with its bottom edge oriented along 040°T.

The OI procedure also estimates the error field for each variable. In this paper, portions of the OI maps are shaded, typically around the periphery of the observational array, to indicate where the mapping errors make features less reliable. Within the unshaded portions of the maps, the Z_{12}^* and P_{3500} fields have accuracies of 39 m and 0.2 kPa, respectively. The deep geostrophic currents at 3500 m agree with measurements within 0.02 m s^{-1}.

Statistical Summary

Transect Time Histories

The meanders and eddies may be initially assessed and their timescales characterized, using the "path" locus, $Z_{12}^*(x, y, t) = 400$ m. This simple description can become ambiguous when meanders are steep or interact with neighboring
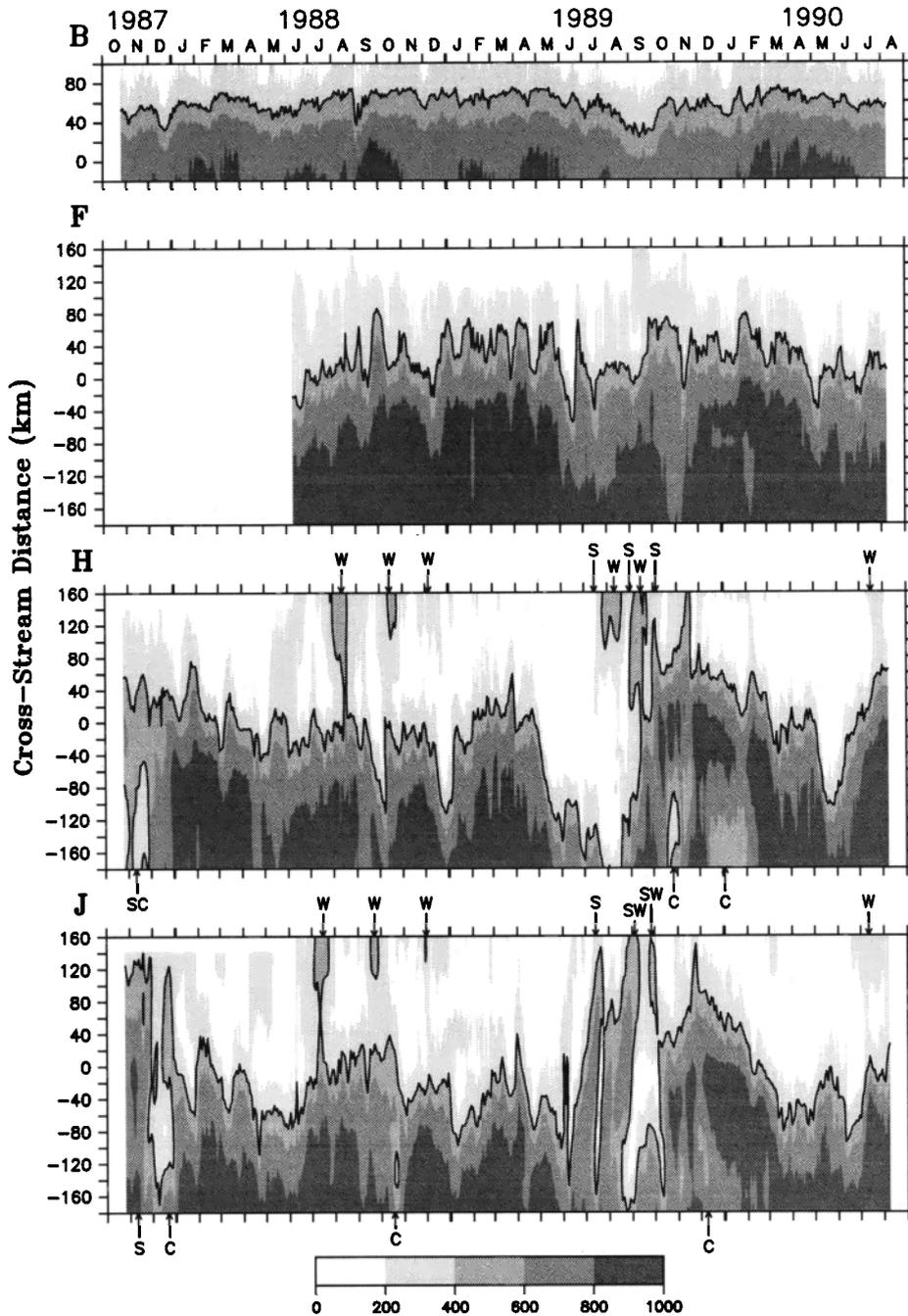
Figure 3. Cross-stream profiles of Z_{12}^* at lines B, F, H, and J for the period October 1987 to August 1990. These time-histories were created by combining Z_{12}^* profiles obtained from the OI maps along fixed grid lines at 2-day intervals, and contoured as functions of cross-stream distance and time. The thermocline depths (in meters) are shaded according to the key at the bottom; shallow Z_{12}^* depths are indicated by white and light gray tones and deep Z_{12}^* depths by darker tones. The solid line highlights $Z_{12}^* = 400$ m. The letters W and C indicate observations of warm and cold core rings, respectively, and "S's" denote periods when the Gulf Stream looped backward onto itself resulting in multiple crossings of the front at the cross-stream line. Cross-stream distance is measured relative to the line origins shown in Figures 5 and 7. Transects are consistent with those shown in Figure 4.

rings. (Here "steep" is used to describe, in plan view, meanders for which the crest-to-trough amplitude is comparable to a half wavelength. Meteorologists would call comparable patterns in the atmospheric jet stream "deep troughs,"

but here the adjective "deep" is reserved for the vertical coordinate.) Along a single transect, the front may even fold back upon itself in an "S-shape".

Figure 3 shows space-time profiles of the Gulf Stream
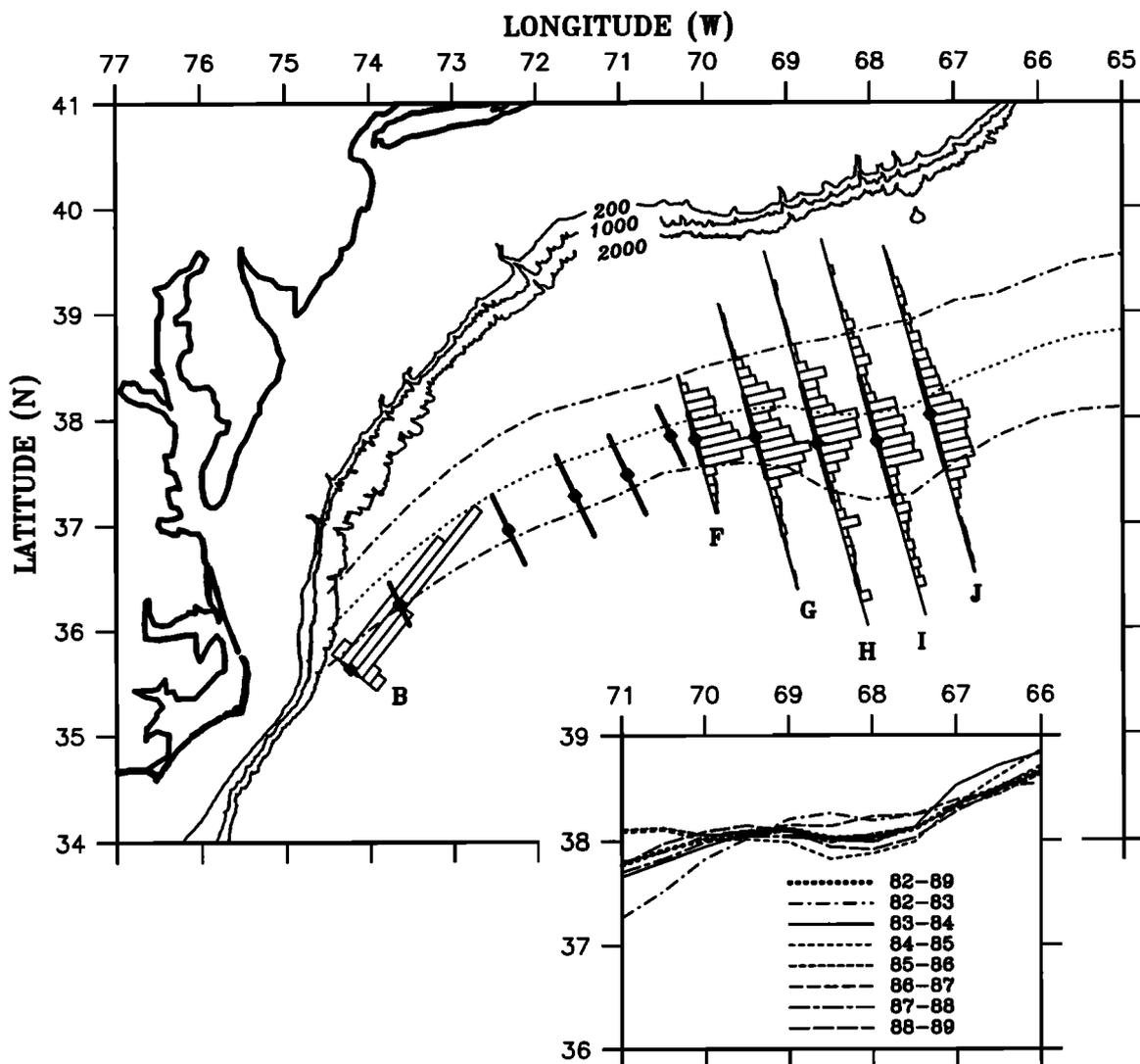
Figure 4. Histograms of the number of daily occurrences of the Gulf Stream position (Z_{12}^* at 400 m depth) within 10-km bins during October 1987 to August 1990. A bar length of 30 min longitude indicates 100 occurrences. End points of the thin lines indicate extreme locations of observed paths. Means and standard deviations are shown by the large diamonds and heavy bars, respectively, along the bases of the histograms. The mean and standard deviations of other IES path data collected during 1982–1986 are also shown. The dotted and dot-dashed lines indicate the mean path and standard deviation, respectively, of the surface front during 1982–1989 supplied by *Lee* [1994]. The inset repeats the 8-year mean surface path, and shows mean paths determined for seven 2-year periods [T. Lee, personal communication, 1994].

thermocline depth on selected transects. The Gulf Stream front in Figure 3 is represented by the shaded contours of Z_{12}^*. Each transect is approximately normal to the mean Gulf Stream, as labeled in Figure 4. Progressing downstream from line B to J, the variability grows in amplitude and complexity.

At line B (74°W) the contours shift nearly in parallel, indicating that the cross-sectional profile remains relatively invariant and the crossing-angle does not change greatly. Meanders occurred on timescales ranging from a few days to several months.

At line F (70°W) despite greater amplitude meanders, the front retains nearly monotonic shoaling of Z_{12}^* northward. The spacing of the contours varies with time, prin-

cipally because the front may cross the transect obliquely. Lateral displacements of about 60 km occur at periods of 25–50 days.

On lines H (68.5°W) and J (67°W) the Gulf Stream front shifts across the full 340-km transect. Z_{12}^* can have local extrema resulting from "S-shaped" paths and from both warm core rings (WCRs) and cold core rings (CCRs). Steep troughs are evident in Figure 3 as large southward displacements. The typical duration of a steep trough is about 1 month, however, the entire summer (May–September) of 1989 is characterized by troughs and "S-shaped" paths.

WCRs (e.g., July-August 1988) appear on lines H and J as isolated pools of deep Z_{12}^* along the northern limit of each transect; they typically cross the transects in 20–

30 days. WCRs were not mapped at line F, because the typical ring track passed northward of the measurements on this longitude. Conversely, CCRs (e.g., October 1989 to January 1990) appear as isolated pools of shallow Z_{12}^* along the southern portion of lines H and J, sometimes transiting and sometimes stalling near 68°W.

Sometimes the Gulf Stream path through the Central Array was relatively straight for periods lasting 3–4 weeks (e.g. February 11, 1989, in Figure 11 shown later). Satellite sea surface temperature (SST) images indicate this typically accompanied long wavelength ($\geq$ 500 km) meanders, such that within the limited mapping window the current appeared relatively unperturbed.

An overall census of events (from OI maps as well as Figure 3) is as follows: Roughly 20 meander crests and troughs with peak to peak amplitudes of at least 50 km propagated eastward through the Central Array during 34 months, sometimes as a wave train of two or three wavelets without exhibiting much growth. Numerous meanders of smaller amplitude ($\leq$ 40 km) passed through the array. Nine steep troughs developed, typically evolving from smaller amplitude eastward-propagating troughs that stalled and steepened. Two of these troughs continued to steepen as they exited eastward, and three others relaxed before exiting to the east. One steep trough formed a CCR directly, and three developed into convoluted "S-shaped" paths before shedding rings. In all, seven WCRs passed through the northern part of the Central Array, with at least two having formed from these "S-shaped" structures. Six of the WCRs interacted or partially coalesced with the Gulf Stream. All four observed CCRs formed within the array; however, three of these never completely separated from

the Gulf Stream. The remaining CCR formed, reattached, and subsequently reformed. This ring, or a portion of it, remained in the Central Array for a 4-month period.

Gulf Stream Path Histograms

Figure 4 charts the probability distribution of the Gulf Stream position (Z_{12}^* at 400 m) along each of six transects, B and F–J. Along each transect the number of days were tallied when the path occurred within a set of 10-km bins; Table 1 indicates the time periods available. Rings were excluded from this tally, and if the path was n-times multivalued on a given day, the contribution to each respective bin was $1/n$. At lines H and I, 20 of the 1017 daily positions were extrapolated beyond the mapped transect: sixteen to the south in steep troughs, and three of the four northward extrapolations in "S-shaped" paths. Only three extrapolations were required at line J, and none at lines F and G. All extrapolated positions were tallied in the respective last bin. The thin line lengths span to the extrema of the observed displacements, as also listed in Table 1. The mean positions ±1 standard deviation are also indicated in Figure 4.

The histogram for line B is representative of all three Inlet Array transects off Cape Hatteras, strongly peaked but becoming progressively broader downstream. Table 1 shows that in the 80 km between lines A and C, the meandering envelope and the standard deviations of the displacements double.

In the Central Array the meander envelope broadens a factor of 2.7 in the 120 km from line F to H. The histogram for line F is peaked, with the central two quartiles spanning 40 km. In contrast at line J the histogram is broader

Table 1. Origins, Orientations, and Deployment Periods for Lines A through J and First Order Statistics (Minimum, Maximum, Mean, and Standard Deviation) of Gulf Stream Displacements for Each Line

Line Designation	Time Period	Number of Observations, days	Line Origin Latitude, N	Line Origin Longitude, W	Line Orientation, T	Displacements Min, km	Displacements Max, km	Displacements Mean, km	Displacements Std, km
SYNOP A	1987–1990	630	35° 00.00'	74° 00.00'	130	36.2	76.1	59.1	7.6
SYNOP B	1987–1990	1053	35° 16.56'	73° 42.06'	130	25.9	79.5	60.7	10.0
	1988–1990	789				25.9	79.5	60.8	10.2
SYNOP C	1987–1990	1053	35° 33.13'	73° 24.23'	130	9.1	90.8	59.9	15.7
	1988–1990	789				9.1	90.8	60.0	15.9
GSDE B	1982–1985	1023	36° 00.00'	73° 30.00'	154	−8.9	77.4	30.3	25.0
GSDE D	1982–1985	1023	36° 33.48'	72° 06.11'	154	−52.0	118.2	47.9	40.1
GSDE E	1982–1985	1023	36° 52.60'	71° 18.18'	154	−84.9	128.2	48.4	46.7
GSDE F	1982–1985	1023	37° 06.95'	70° 42.22'	154	−82.7	121.1	43.0	45.5
GSDE G	1983–1986	1000	37° 21.30'	70° 06.27'	154	−33.2	125.0	58.9	34.0
SYNOP F	1988–1990	789	37° 34.82'	70° 01.30'	165	−54.4	88.7	25.3	27.9
SYNOP G	1987–1990	1017	37° 43.21'	69° 20.87'	165	−145.3	156.3	11.8	44.8
	1988–1990	789				−145.3	156.3	10.4	46.5
SYNOP H	1987–1990	1017	37° 51.61'	68° 40.43'	165	−210.6	197.0	−11.6	64.4
	1988–1990	789				−210.6	197.0	−18.3	70.2
SYNOP I	1987–1990	1017	38° 00.00'	68° 00.00'	165	−216.0	194.2	−25.5	69.9
	1988–1990	789				−216.0	194.2	−32.7	73.5
SYNOP J	1987–1990	1017	38° 08.39'	67° 19.57'	165	−179.3	170.1	−12.7	59.6
	1988–1990	789				−179.3	170.1	−9.3	60.6
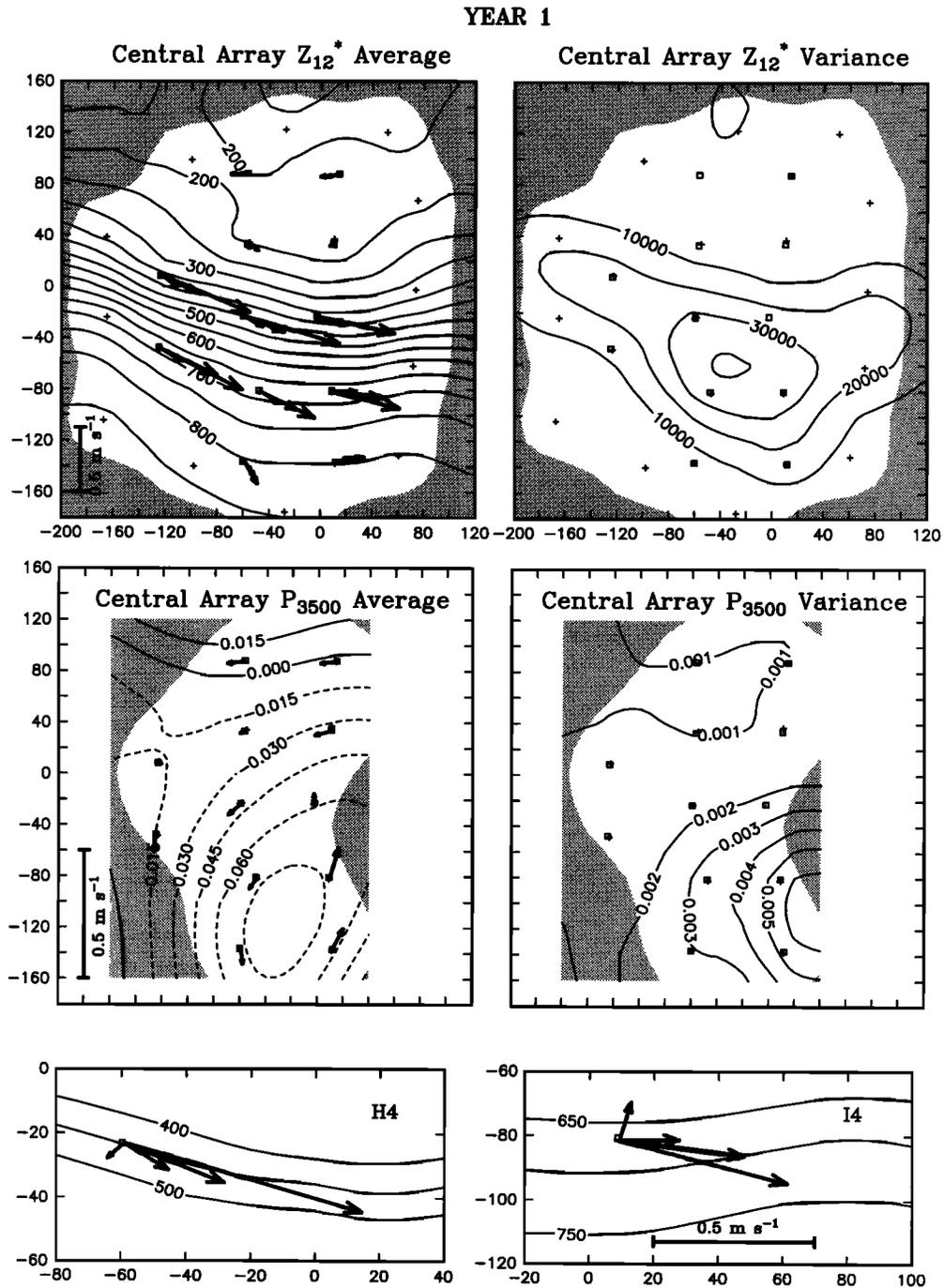
Figure 5. Mean and variance fields for Year 1, June 15, 1988 to May 27, 1989. Left-hand panels show the mean Z_{12}^* and P_{3500} fields of the Central Array. Contour intervals are in meters for Z_{12}^* and decibars (where 1 dbar = 10 kPa) for P_{3500}. Right-hand panels show the corresponding variance fields in units of meters-squared and decibars-squared for Z_{12}^* and P_{3500}, respectively. Each frame corresponds to the boxed region near 68°W shown in Figure 2. The distances (in kilometers) are referenced to the grid origin at 38°N, 68°W with x-axis oriented along 075°T. Shading indicates regions where the estimated mapping errors are high. IES sites are denoted by plus symbols and current mooring sites by open squares. Averaged current vectors at 400, 700, 1000 m are superimposed on the Z_{12}^* field, and the average 3500 m currents on the P_{3500} field. A speed key is indicated for each plot. For consistency, all quantities have been averaged over the same time period. Bottom row shows expanded plot of all four levels of mean currents at sites H4 and I4.
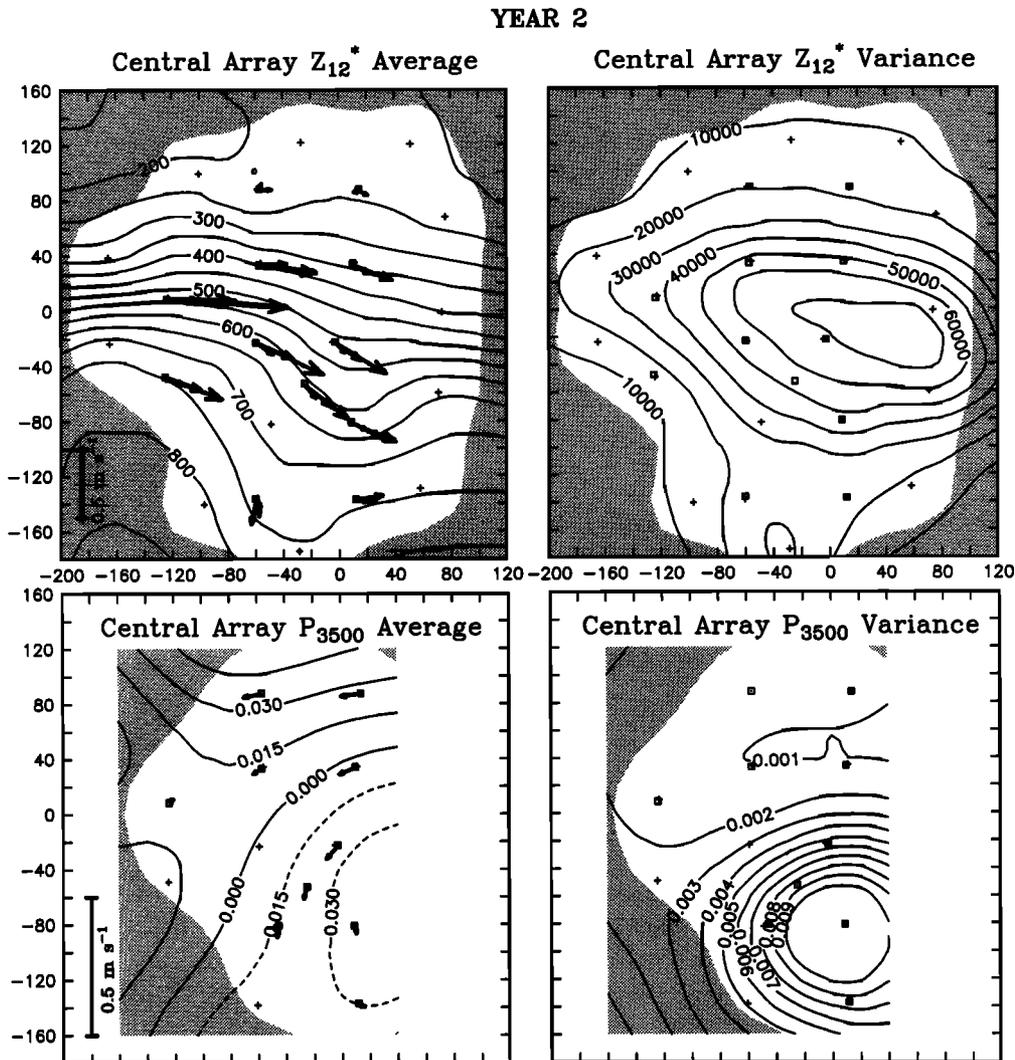
YEAR 2

Figure 6. Same as top two rows in Figure 5 except for Year 2, August 28, 1989 to August 7, 1990.

and more uniform, with a quartile range of 80 km. This downstream change in displacements and histograms occurs smoothly from lines F–J. The weak modes on lines G, H, and I are not statistically significant.

Means and Variances of the Thermocline and Deep Pressure Fields

The time-averaged fields at the thermocline and deep levels are presented for two convenient 1-year periods in this section. Year 1 is June 15, 1988 to May 27, 1989, and Year 2 is August 28, 1989 to August 7, 1990. (The selection of these two time periods was dictated by the failure of both IESs on line A at Inlet Array during June 1988 to August 1989.) These two averaging periods serve the purpose of contrasting years of relatively quiet versus relatively energetic meandering. Although there is substantial interannual variability, the basic features are robust when averaged over a year. (Current velocity, Z_{12}^*, and P_{3500} averages for the full 26-month time period in the Central Array are presented in Part 2.)

Central Array Z_{12}^*. Figures 5 (Year 1) and 6 (Year 2) show the average Z_{12}^* and P_{3500} fields for the Central Array.

Superimposed on the Z_{12}^* fields are the average current vectors at the 400, 700, and 1000 m levels; the 3500 m average current vectors are on the P_{3500} fields (stretching the scale). In the right-hand column of these figures are variance fields of Z_{12}^* and P_{3500}.

During both years the mean Z_{12}^* field had a weak trough. However, the mean cross-frontal slope of the thermocline was considerably sharper in Year 1 than in Year 2, because of the latter's more vigorous meandering (cf., Figure 3). In Year 1, the mean Z_{12}^* field reversed slope and deepened slightly in the north ($y > 80$–100 km) due to the presence of warm core rings.

The mean upper level current vectors align well in these figures with the direction of thermal wind indicated by the mean Z_{12}^* front, such that at leading order they would be described as "equivalent barotropic." However, close examination reveals that the currents turn systematically with height at some sites. The average currents at all four levels at two mid-Gulf Stream sites are expanded in the panels at the bottom of Figure 5. The currents at site H4, leading into the trough, turn counterclockwise with increased height (backing), and the currents at site I4, exiting the trough, turn clockwise with height (veering). The turning

at both sites exceeds the combined rms errors of measurement and mooring-motion compensation.

The Z_{12}^* variance fields for Year 2 were nearly a factor of 2 larger than for Year 1 (except at $x \sim -160$ km, the 70°W "node", where they were about the same). The Year 1 variance was largest under the steepest portion of the mean front, arising simply from meandering of the front during the averaging period. However, the Year 2 variance was distributed more broadly, having arisen from the greater diversity observed in Gulf Stream paths and adjacent eddies during Year 2.

The average Z_{12}^* field was also determined for "Year 0" (October 26, 1987 to June 14, 1988), when only the IESs were deployed (not shown). A mean trough was evident during that period as well, and the variance was slightly greater than Year 1.

Central Array P$_{3500}$. Careful examination of the P_{3500} mean fields for the 2 years shown in Figures 5 and 6 reveals many similarities between them. In both years, in the northern portion of the maps, the mean deep currents shoreward of the 4000-m isobath (sites H2 and I1) flowed westward approximately following the bathymetry. An abyssal mean cyclone was present both years in the southeastern portion of the maps. The low-pressure center shifted to the east about 60 km in Year 2 (as did the mean upper layer trough also). The DWBC, confined shoreward of the 4000-m isobath, and the deep cyclone were features also seen in earlier studies reported by *Luyten* [1977] and *Watts* [1991]. The total range of the mean bottom pressure field was about 0.9 kPa for both years.

The P_{3500} variance for Year 2 was nearly double that for Year 1 (similar to the ratio of the upper layer variances). The maximum variance of P_{3500} was offset southward from the maximum variance of Z_{12}^*.

In both years the mean abyssal cyclones were offset downstream from the mean upper layer troughs by about 20 to 40 km. If the wavelength is approximately 320 km, the corresponding phase shift vertically is about $\pi/8$ to $\pi/4$. The sense of this phase shift corresponds to the theoretical signature of baroclinic instability, involving interaction of the abyssal and upper layer flow [*Holton*, 1979]. Under this scenario, the coupling is effected via vertical stretching as the front meanders. These processes will be illustrated later in this paper and in Part 2, however their dynamical balances are beyond the scope of this overview.

Inlet Array Z$_{12}^*$. The Year 1 and Year 2 mean Z_{12}^* fields for the Inlet Array are shown in Figure 7. The mean fields had only subtle differences between the years. From Year 1 to Year 2, the mean location and angle of flow of the Gulf Stream shifted about 10 km and rotated about 10° offshore on line B. (These changes can also be noted in the time series shown later in Figure 9.)

The associated Z_{12}^* variance fields in the Inlet Array are included on Figure 7. The variance roughly doubles from line B to C during both averaging periods, while increasing by more than a factor of 3 from Year 1 to Year 2. The Inlet Array mean and variance fields were also determined for the period October 1987 to June 1988 (Year 0, not shown); the mean path resembled Year 2, but the variance

Year 1

Year 2

Z_{12}^* Average Z_{12}^* Variance
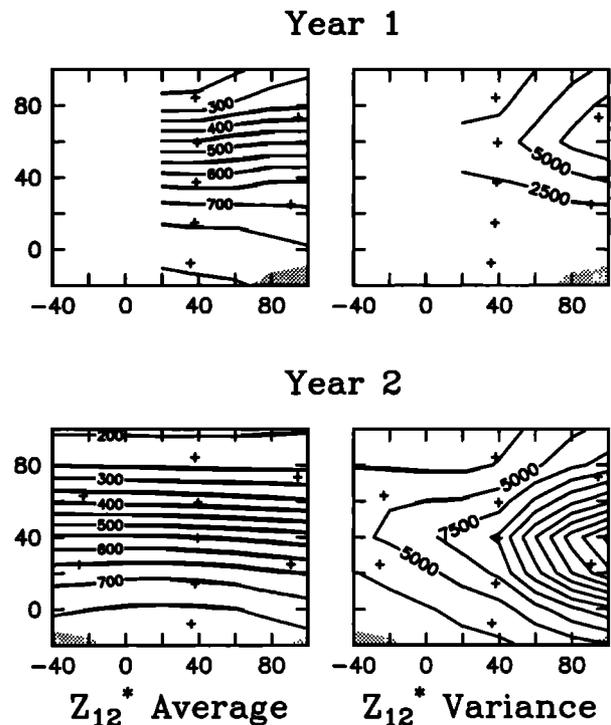
Figure 7. Same as Figure 5 except only for the Inlet Array Z_{12}^* mapping region and including both Year 1 and Year 2. The mapped Z_{12}^* field during Year 1 does not extend as far upstream as during Year 2 because both IESs along the A line failed that year.

was only slightly greater than during Year 1. These interannual differences at the Inlet Array are intriguing because they appear to be reflected in the Central Array variability. For example, during Year 2 when the Inlet Array variance field was the largest, the Central Array variance field was also the greatest.

Spectral Characteristics of the Displacements

To produce single-valued time series of path location, rings were excluded and the few multivalued events were identified by eye to select one crossing per day. The path-meander spectra on lines B and F–J are shown in Figure 8 (note the ordinate scale change). All spectra were computed using of the Welch method [*Little and Shure*, 1993], breaking the records into Hanning-windowed and overlapped 256-day segments and ensemble-averaging the individual spectral estimates. Subsequently, the higher frequency estimates were band-averaged to produce spectral estimates with between 8 and 136 degrees of freedom, depending on frequency. The spectra are plotted in variance-conserving form in Figure 8, together with their 95% confidence limits. The total variance increases eightfold between lines B and F and increases an additional sixfold between line F and lines H and I. The variance subsequently decreases about 14% between lines I and J.

Near 74°W on line B the spectrum is basically red with slightly higher energies at 128-day, 25- to 50-day, and 6- to 8-day periods. It is similar in shape and magnitude to that
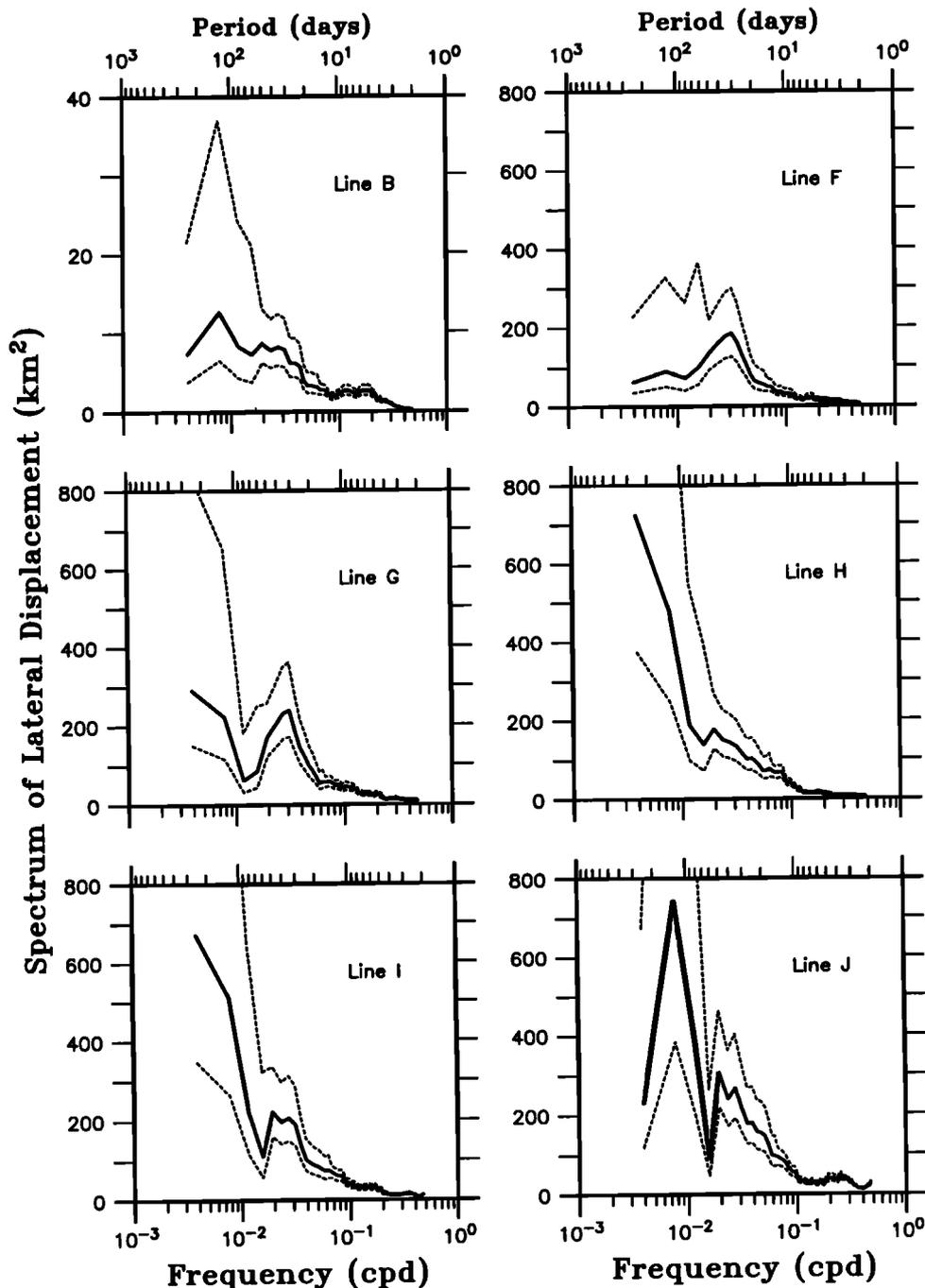
Figure 8. Variance-conserving spectra of path displacement at line B in the Inlet Array and lines F–J in the Central Array. All spectra were produced using 34 months of data except line F for which only 26 months were available. The 95% confidence intervals are indicated by the dashed lines. Due to the plotting scale chosen the upper limits for the spectral estimates at 256- and 128-day periods are not shown; for these two lowest frequencies the upper confidence limit is a factor of 2.9 times the respective spectral estimate.

found by *Tracey and Watts* [1986], for a similar location (their line A) during 1979–1982.

In all six spectra, a peak is present at periods of 20–50 day. Although the statistical confidence limits indicate that it may not be a distinct peak, they confirm a plateau of increased spectral variance in that period band. The energy associated with this peak increases more than tenfold

between 74°W (line B) and 70°W (line F), and then remains relatively constant to 67°W.

The long-period meanders, roughly 85 days or longer, exhibit important qualitative spectral changes downstream through the Central Array. The low total variance near 70°W (line F), and its narrow histogram (node) seen in Figure 4 are due to the relative lack of long-period variance.

In contrast, meanders on lines H, I, and J have most of their variance associated with longer periods (i.e., $\geq$ 128 days). At the longest period resolved (256 day) line J had substantially less variance than lines H and I. The low-frequency spectral changes from line H–J apply during this set of observations, but may not necessarily represent the longer-term average.

Lastly, the short period band (4–5 days) at line J has significantly increased variance over that of lines F–I, suggestive of the growth of secondary instabilities on the larger-scale meandering front. An example is shown later of short-wavelength meanders riding on a longer-wavelength meander.

Discussion of the Statistical Summary

For comparison, additional statistics on the path of the Gulf Stream at the surface and 400 m, from Cape Hatteras to 67°W appear in Figure 4 and Table 1. These additional values come from different data sources during different time periods. The digitized positions of the satellite-derived SST front averaged over the 8-year period 1982–1989 were provided by *Lee* [1994]. Gulf Stream position statistics are included from IESs on five lines between 74°W and 70°W during an earlier experiment (1982–1986). Note that the offsets shown between the mean surface and subsurface front do not indicate the true offshore tilt, because the sampling days differed, the averaging time periods differed, and the transect lines were not colinear.

An important point to be drawn from the information in Figure 4 is that the mean path and meandering envelope for the 2-year SYNOP experiment is representative of the typical 2-year pattern and the long-term average. In particular, the trough in the mean Gulf Stream path near 68°W is a recurring pattern, exhibited in five of the seven 2-year mean paths shown in the inset. Moreover, *Halliwell and Mooers* [1983] examined the Gulf Stream path during 1975–1978 and also found that the mean path of the surface front had a weak trough at 68°W.

The node near 70°–69°W has also been reported by other investigators [*Cornillon*, 1986; *Gilman*, 1988; *Kelly*, 1991]. *Halliwell and Mooers* [1983] found a local minimum in the overall standard deviation of the surface path between 71°–70°W. Recent work by *Kontoyiannis and Watts* [1994] and *Lee* [1994] offer reasons for the existence of the node. The latter shows that because a retrogressive tendency on phase speed arises for large-amplitude meanders [*Cushman-Roisin et al.*, 1993], wavelengths around 1000 km can form standing modes with one node clamped near Cape Hatteras and another one-half wave downstream, near 70°–69°W. The spectra discussed with Figure 8, in the semi-annual to annual band, are consistent with standing meanders of this wavelength and a node near 70°–69°W.

Thermocline Structure and Dynamical Processes

The Front Near Cape Hatteras

At the Inlet Array, Gulf Stream variability is usually characterized by near-sinusoidal, small amplitude meanders. Because meanders propagate downstream from this region and grow, these data may provide upstream boundary conditions for statistical and dynamical modeling, as in *Cronin et al.* [1992a] and *Kim* [1994], respectively. The latter assimilated the inflow streamfunction and vorticity $(\psi, \nabla^2 \psi)$ in an equivalent barotropic model and verified it in the Central Array. For illustration, Figure 9 shows time series of position, angle, and curvature of the path at line B. Curvature κ was determined approximately where the mean stream center, $Z_{12}^* \sim 400$ m, crossed line B. For a surface $Z(x, y)$ spline-fitted to the OI Z_{12}^* field with derivatives indicated by subscripts, curvature was calculated as

$$\kappa = \frac{- \begin{vmatrix} Z_{xx} & Z_{xy} & Z_x \\ Z_{yx} & Z_{yy} & Z_y \\ Z_x & Z_y & 0 \end{vmatrix}}{(Z_x^2 + Z_y^2)^{\frac{3}{2}}}$$

[*Bronshtein and Semendyayev*, 1985] where positive path curvature is cyclonic. The five OI maps across the bottom illustrate three of the largest meander perturbations.

The position of the front typically shifted less than 5 km from day to day. The front generally followed a course of 038°–047°T, typically varying by less than 10° from day-to-day. In extreme cases the front changed position by 15 km and angle by 25° in a day (e.g., September 1988).

The first three OI maps, selected from a late December 1987 event, reveal a short wavelength meander propagating northeastward. During this event κ varied between -0.007 km^{-1} and $+0.01$ km^{-1}, so $|\kappa v|$ is about 8–12% of f (for $v \sim 1$ m s^{-1}).

The largest deflection offshore lasted from August to October 1989, during which time the front also assumed its most eastward angle, 073°T. Observations in the Central Array and satellite SST images revealed that the Gulf Stream path east to at least 67°W was highly convoluted during this same period. The largest negative $\kappa \sim -0.014$ km^{-1} occurred during this event (with $|\kappa v| \sim 17\%$ of f), turning the current further from its mean path.

In January 1990, the path shifts about 20 km onshore in a propagating meander crest. The large negative $\kappa \sim -0.01$ km^{-1}, turns the current toward its mean position, with $|\kappa v| \sim 12\%$ of f.

Effects of Path Curvature on Thermocline Structure

The synoptic cross-sectional profile of velocity and temperature in the Gulf Stream is remarkably constant from 74°W to 67°W [see *Halkin and Rossby*, 1985 and *Johns et al.*, 1995]. Nevertheless, systematic variations in structure have been reported [e.g., *Manning and Watts*, 1989], and in particular *Hansen and Maul* [1970] and *Horton* [1987] report that the steepness of the thermocline slope varies with κ.

In the Central Array Z_{12}^* maps, the front tends to broaden in meander crests and narrow in troughs. (An illustration of this is the March 29, 1989 map in Figure 11, in which both a crest and a trough are evident.) The following demonstrates that the dependence of the cross-stream profile of thermocline depth, $Z_{12}^* = h(n)$, upon path curvature is approximately consistent with simple gradient wind balance:
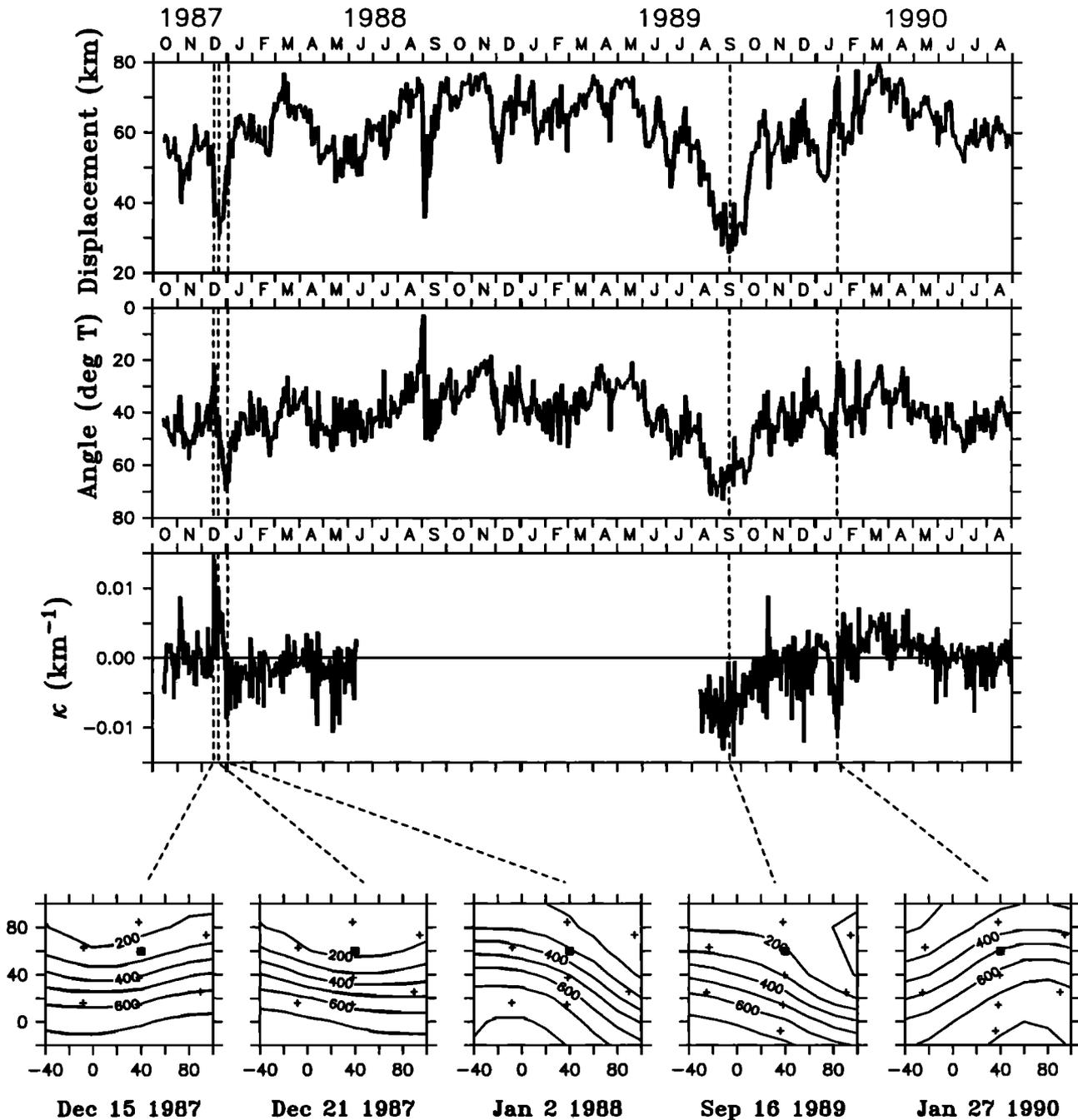
Figure 9. Gulf Stream path parameters, position, angle and curvature κ, at line B are shown as functions of time for the period October 14, 1987 to August 31, 1990. No κ estimates are shown for the period June 1988 to August 1989 when the line A data were missing. Examples of five thermocline depth fields for the Inlet Array are shown in the bottom row. Displacements are measured relative to the origin of the cross-stream line at $x = 40$ km. The path angle was calculated as the direction of $Z_{12}^* = 400$ m between lines B and C relative to true north, and κ was determined at the location marked by the square in the Z_{12}^* fields. Vertical bars through the time series indicate the dates of the five Z_{12}^* fields shown. The Z_{12}^* contours are in meters. Each frame corresponds to the small boxed region near 74°W shown in Figure 2, with the x-axis oriented along 040°T and distances in kilometers from 35°N, 74°W.

$$\kappa V^2 + fV = -\frac{1}{\rho}\frac{\partial p}{\partial n} = g^*\frac{\partial h}{\partial n} \qquad (1)$$

The cross-stream pressure gradient is expressed as the cross-stream slope of the thermocline $\partial h/\partial n$ times a reduced gravity, and is balanced by Coriolis and centrifu-

gal accelerations $(fV, \kappa V^2)$. For $\kappa = 0$, (1) simplifies to $fV_0 = g^* (\partial h/\partial n)_0$.

Assuming that along-streamline pressure gradients are weak and do not significantly accelerate the flow then the velocity along a streamline is nearly constant, $V = V_0$. Although higher order effects perturb parcel velocities in all

three dimensions (cross-stream, vertical, and alongstream), particularly in steep meanders, this useful assumption (see *Palmén and Newton* [1969]) is approximately borne out by the results in this section.

Under this assumption (1) can be rearranged to give

$$\frac{\partial h}{\partial n} = \left(\frac{\partial h}{\partial n}\right)_0 \left[1 + \kappa \left(\frac{\partial h}{\partial n}\right)_0 \frac{g^*}{f^2}\right] \qquad (2)$$

predicting a linear dependence of thermocline slope upon κ. According to (2) the spacing (δn) between h contours decreases in the troughs and increases in the crests.

Relationship (2) was tested with a set of Z_{12}^* maps representing the range of Gulf Stream path curvature. The maps were categorized according to five curvature classes: strong and moderate negative ($\kappa \leq -0.014$; and $-0.014 < \kappa < -0.007$), straight ($-0.007 \leq \kappa \leq +0.007$), and moderate and strong positive ($+0.007 < \kappa < +0.014$; and $\kappa \geq +0.014$) (units: (km^{-1}). These classes were chosen such that $|\kappa| \, V/f$ is $> 10\%$ for the strong cases, 5–10% for the moderate cases, and $< 5\%$ for the straight paths.

For each selected map, the profiles $Z_{12}^* = h(n)$ were determined along transects perpendicular to the current. Sixteen profiles were selected to represent $\kappa = 0$, and nine profiles represented each of the other four curvature classes (52 dis-

tinct cases altogether). Within each κ class the mean profile $h(n)$ was determined, with standard deviation $\delta h(n)$.

Figure 10 plots the thermocline slopes $\partial h/\partial n$ versus κ at several depth levels across the mean section. For all depths, the slopes tend to steepen with more positive curvature, being 30–60% steeper for the strong positive κ case than for the strong negative κ. Figure 10 also lists the correlation coefficients (r) for linear regression of $\partial h/\partial n$ on κ. Values for depths from 350 to 550 m are significant at the 98% confidence level. The correlation coefficients at $Z_{12}^* = 250$ m and 650 m are significant at the 90–95% level, somewhat lower because eddy variability on the edges of the Gulf Stream has a greater effect upon the gentler slopes that exist there.

A quantitative examination of (2) can be made by using a value $g^* = 1.53 \times 10^{-2}$ cm s^{-1} from *Kim and Watts* [1994], appropriate for 400 m and the observed $\left(\partial h/\partial n\right)_0$ of 6.6×10^{-3} at 450 m. The slopes predicted for $\kappa = 0.014$ and $\kappa = -0.014$ are respectively 7.8×10^{-3} and 5.4×10^{-3}, which agree with the observed slopes within 5%. The data throughout the strong central front support the above simple theory for the curvature dependence of the cross-stream slope of the thermocline.

Case Studies of Meander Structure

Processes near 68°W are exemplified by the upper level and deep maps shown in the paired set of Figures 11 and 12. To facilitate comparisons, coarsely contoured Z_{12}^* fields are superimposed on the P_{3500} maps in Figure 12. Corresponding current vectors are plotted at the mooring sites in each frame. In Figure 11 the currents at the upper three measurement levels (400, 700, and 1000 m) may be distinguished because the velocity increases upwards. In Figure 12 the 3500 m currents are shown with double the vector length scale of Figure 11, because the abyssal currents are usually considerably weaker than those at 400 m. The velocities at 3500 m are, at times, stronger than those at 1000 m.

Six distinct Gulf Stream paths and eddy interactions are illustrated in the figures: (1) a relatively simple straight path and weak abyssal flow, (2) a steep meander crest and abyssal anticyclone, (3) a steep elongated meander trough and strong abyssal cyclone, (4) a warm core ring (WCR) north of the Gulf Stream front, (5) a convoluted "S-shaped" path in which the Gulf Stream loops back, with an abyssal cyclone and anticyclone, and (6) a cold core ring (CCR) south of the Gulf Stream. Part 2 illustrates the time development of two of these cases, and detailed case studies are the subject of articles in preparation.

The deep layer exhibits great variability as the upper front meanders. When the upper layer jet flowed along a relatively straight course, the P_{3500} fields were sometimes essentially featureless with deep currents weaker than 0.05 m s^{-1}. However, whenever the Gulf Stream path meandered vigorously, the P_{3500} fields exhibited low-to-high ranges up to 4 kPa across the array, and the deep currents were organized into anticyclones and cyclones with speeds sometimes exceeding 0.40 m s^{-1}.

The strength of the deep currents is noteworthy because they far exceed the common perception of weak abyssal
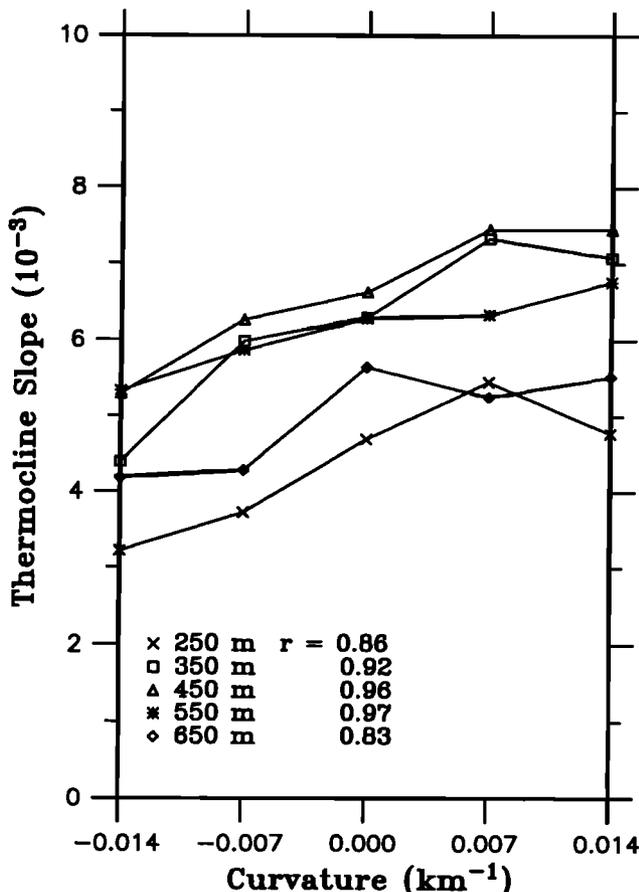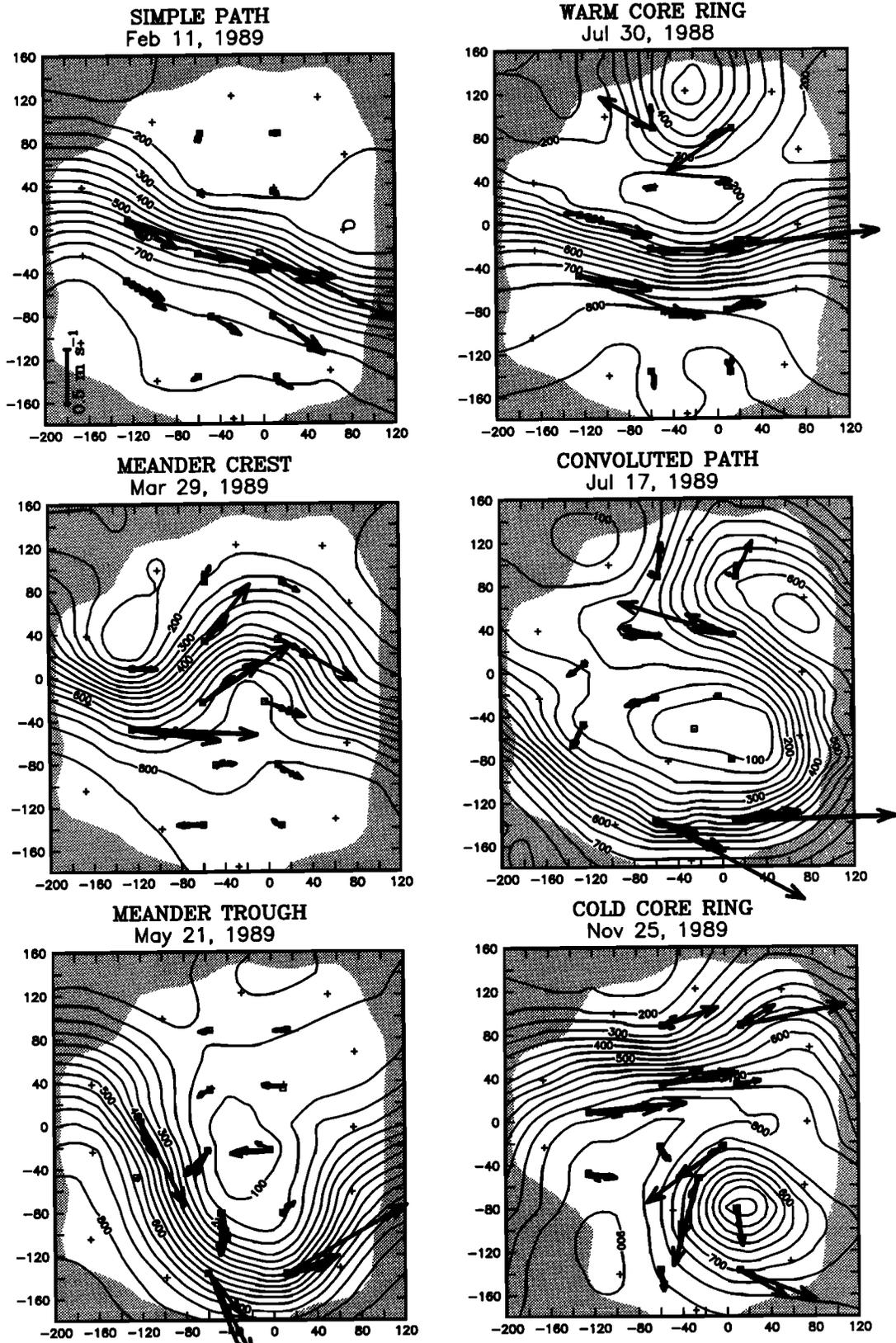

Figure 10. The slope of the thermocline $\partial h/\partial n$ measured at depths 250–650 m are plotted versus curvature κ. Correlation coefficients r for the linear regression of $\partial h/\partial n$ on κ are listed for each depth level.

Figure 11. Six different event maps of the depth of the 12°C isotherm (Z_{12}^+) showing the Gulf Stream and the neighboring eddy field in the Central Array. The Z_{12}^+ fields are contoured at 50 m intervals and the shading indicates regions where estimated mapping errors are high. Vectors show the measured currents at 400, 700, and 1000 m depths, distinguishable because the speed increases upwards. In all cases the vectors indicate the 40-hour low-pass filtered velocity at the time of the OI map. (upper left) The vector length scale applies to all six panels.
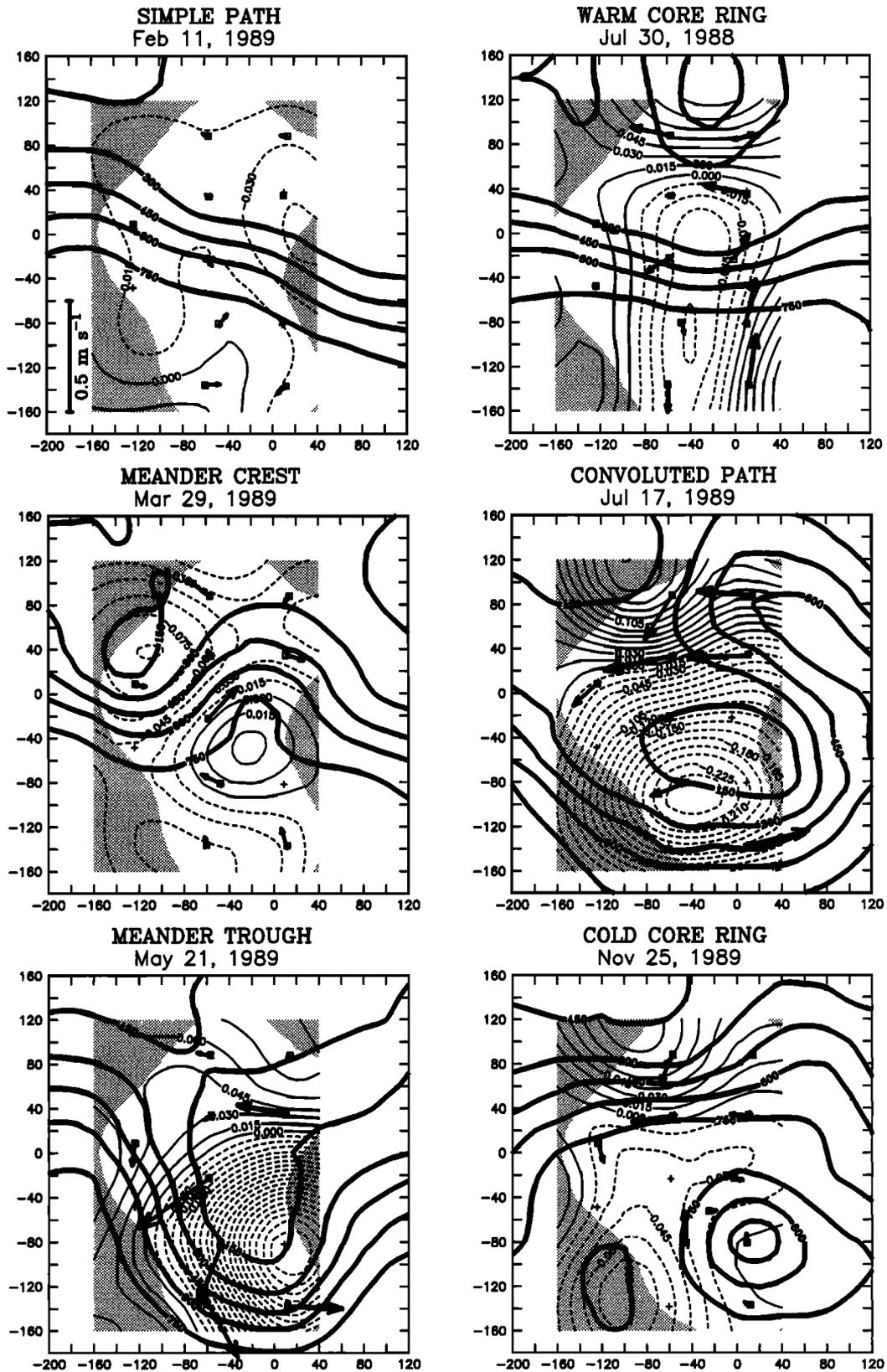
Figure 12. Deep pressure (P_{3500}) fields for dates corresponding to those shown in Figure 11. Bottom pressure measurements were obtained at all 12 sites. Current measurements at 3500 m were obtained at sites with vectors that indicate the 40-hour low-pass filtered current on that day. (upper left) The vector length scale applies to all six panels. The contour levels of the demeaned P_{3500} are in decibars (10 kPa = 1 dbar) and mapping regions with high errors are shaded. The Z_{12}^* fields are repeated from Figure 11, except using bold contours at coarse 150 m intervals.

currents under the Gulf Stream. However, *Schmitz et al.* [1970] and *Luyten* [1977] also report observing peak deep currents of O(0.40 m s^{-1}) under the Gulf Stream near 70°W. Additionally, *Hall and Bryden* [1985] observed speeds up to 0.30 m s^{-1} in a year-long record at 68°W.

February 11, 1989. The Gulf Stream followed a fairly straight path, and the upper level currents were aligned with the front (Figure 11). The upper jet flowed to the east through the array as part of a long-wavelength trough that satellite SST images showed to extend about 390 km downstream. Moreover, the P_{3500} field (Figure 12) was nearly uniform with a total range of only 0.6 kPa. The low P_{3500} values ($P_{3500} \leq -0.3$ kPa) to the east were probably the deep signature of the upper level long-wavelength trough.

Upon close inspection, a small amplitude ($\sim$ 20 km) meander is visible in the Z_{12}^* field, with $\lambda \sim 140$ km and a crest near $x = 0$. This may be an example of a secondary instability developing on the long wavelength meander. Other features moved in to obscure it in less than 7 days, but while it could be traced, the propagation speed of this short-wave feature was approximately 14 ± 3 km d^{-1}.

Another reason for showing this simple example is to dispel the impression that strong events and flows were "always" occurring, an impression which might otherwise be gained from concentrating solely on the other five events shown here.

March 29, 1989. The Gulf Stream had a large amplitude wave with wavelength $\lambda \sim 300$ km and peak-to-peak amplitude > 80 km. This steep crest propagated rapidly at about 18 ± 5 km d^{-1} through the Central Array as part of a train of three successive crests. The P_{3500} field exhibited an anticyclone-cyclone pair directly below the upper trough-crest pair. Consequently, the currents at all levels were well aligned with the baroclinic front, characteristic of an equivalent barotropic current structure. Part 2 presents a series of Z_{12}^* and P_{3500} maps detailing the development of this event over a 24-day period.

May 21, 1989. A steep trough developed together with an intense deep layer cyclone. The currents at 3500 m reached extreme speeds of 0.45 m s^{-1}. The deep flow is not aligned with the baroclinic front, but instead crosses the upper layer flow at large angles at most of the sites.

The temporal development of this trough, which is illustrated in Part 2, was representative of the other steep troughs observed. Each case began with a small-amplitude upper layer trough and a lower layer cyclone that jointly intensified. A detailed dynamical study of deep layer cyclone development and coupling to upper layer troughs is being undertaken [*Savidge and Bane*, 1994]. The center of this deep layer cyclone was downstream of the upper layer trough, roughly by one-eighth wavelength. The sense of the vertical tilt of the pressure fields was opposite to that of the vertical shear of the mean current, providing a characteristic signature of baroclinic instability.

July 30, 1988. A WCR was observed in the northern portion of the Central Array (Figure 11). This ring passed slowly westward ($\sim$ 4.3 km d^{-1}) with only weak indications of interaction with the Gulf Stream. Beneath the WCR, the observed portion of the P_{3500} field (Figure 12) increased to the north, and the deep currents were to the west.

In addition, an elongated deep pressure low extended across the Gulf Stream. However, this should not be taken as a "typical" deep pressure pattern associated with WCRs. In selecting cases to show it was in fact difficult to typify the P_{3500} fields when rings passed through the Central Array. Instead, the deep pressure fields were quite varied and often complex.

July 17, 1989. The development and evolution of this event could be traced from a steep trough in late June. By this date, the Gulf Stream had looped back to create an "S-shaped" path, and the deep pressure field developed a strikingly intense cyclone under the trough and intense high pressures just northeast of the crest. The deep currents reached speeds of about 0.30 m s^{-1} at several sites. In the northern portion, strong westward flow at 3500 m exists between the low and high pressure centers. The direction of this deep flow is suggestive of further intensification and evolution of the upper meander crest. In fact in late July, subsequent to the date shown, a WCR formed.

November 25, 1989. As the culmination of the period of vigorous meandering noted in Figure 3 for May–November 1989, by late November a CCR had fully separated from the Gulf Stream. During these months the pattern of the front progressed twice through the sequence of steep trough/crest development, convoluted "S-shaped" path, and formation of closed warm and cold core ring circulations that recoalesced into the Gulf Stream. The May 21, and July 17, 1989 maps are representative examples of that sequence of events.

The process of ring separation, which occurred during the week of November 13–20, is treated in the next subsection. The CCR is shown in the November 25 map (Figure 11) after it had fully separated from the Gulf Stream; it stayed within the Central Array and remained separated for four months.

The P_{3500} field on this date (Figure 12) suggests a cyclone offset westward from the upper level cyclonic ring center. However, no single pattern can represent the P_{3500} field for this time period, because it exhibited a series of highs and lows that propagated westward through the region, beginning in October and lasting through late December 1989. These deep eddies may be identified tentatively from their observed wavenumber, frequency, and kinematics as topographic Rossby waves, which appear to have originated somewhere farther to the east. They appear to play an important role in modulating, via cross-frontal advection, the upper layer ring formation and ring stream interactions, but it is beyond the scope of this paper to treat this further.

Ring Formation Event

Plates 1 and 2 present the CCR formation process on November 13, 1989, in broad plan view and in a three-dimensional perspective view. Plate 1 shows a satellite SST image of the Gulf Stream together with the Z_{12}^* maps from the Inlet and Central Array IESs. Superimposed on it are the current vectors at 400 m for the same date. Even
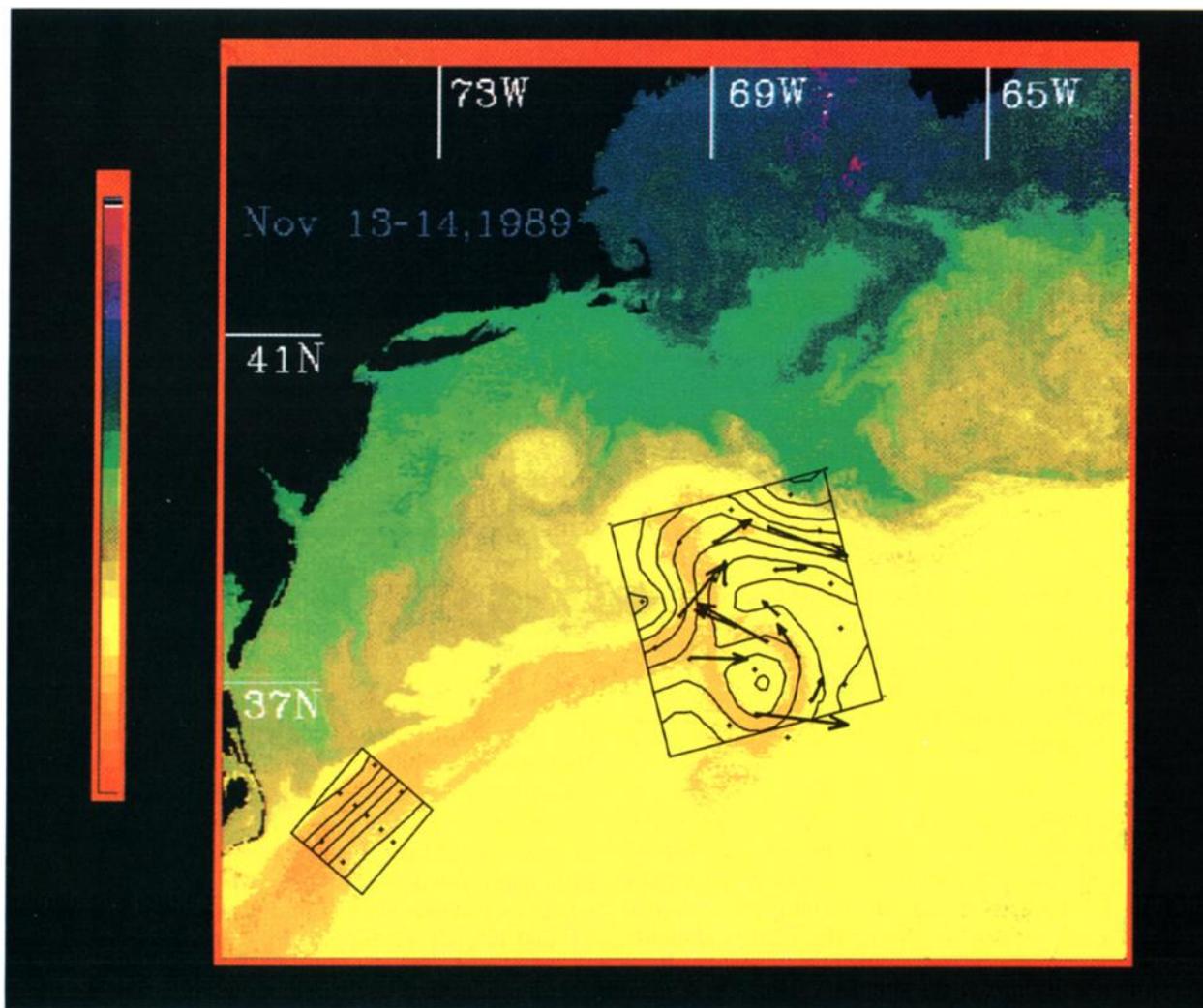
Plate 1. Satellite-derived composite SST field for November 13–14, 1989, (supplied by P. Cornillon). Temperatures in the color bar range from 0°C (magenta) to 30°C (orange). The Z_{12}^* fields for the Inlet and Central Arrays on the same date are superimposed on the SST image; the contour interval is 100 m. Z_{12}^* ranges from less than 200 m in both arrays to more than 700 m and 800 m in the Inlet and Central Arrays, respectively. Currents at 400 m are indicated by the vectors; the longest vector indicates a current speed of 1.37 m s^{-1}.

in this perturbed situation, in which the elongated neck of a steep trough is pinching together to form both a CCR and a steep crest, the SST, Z_{12}^*, and current measurements correspond well. For instance, the warm core of surface water carried by the swiftest currents near the center of the Gulf Stream splits to flow around the ring and along the remaining portion of the Gulf Stream. The Z_{12}^* field confirms that some contours are closed and others remain open around the nascent ring at this date.

The IES Z_{12}^* fields may alternatively be interpreted as dynamic heights, acting as streamfunctions for the upper layer geostrophic flow (see *Kim and Watts* [1994] and *He* [1993]). The dynamic height of the sea surface is indicated on Plate 2 as a raised mesh.

Superimposed on the surface dynamic height mesh are the same satellite SSTs as in Plate 1. (The different color palette from Plate 1 was chosen to represent temperatures

throughout the water column.) The surface warm core follows the inclined portion of the dynamic topography, and the cold core coincides with a cyclonic low at the surface.

All elements of this perspective view of the Gulf Stream are constructed from observations. Streamfunctions ψ optimally mapped from the current meter measurements indicate the trough neck pinching and beginning to form closed-ring contours also at 400, 700, and 1000 m. The temperature fields, mapped in color from independent measurements at each level, indicate dynamically significant offsets from the ψ contours. Heat advection accompanies the upstream offset of the cold and warm temperature centers relative to the respective low- and high-pressure centers. The phase shift between the T and ψ fields, by 20–40 km in a feature of 300-km wavelength ($2\pi/16$ to $2\pi/8$) has the sense of textbook examples of baroclinic instability [e.g., *Holton*, 1979]. The phasing is consistent with a growing
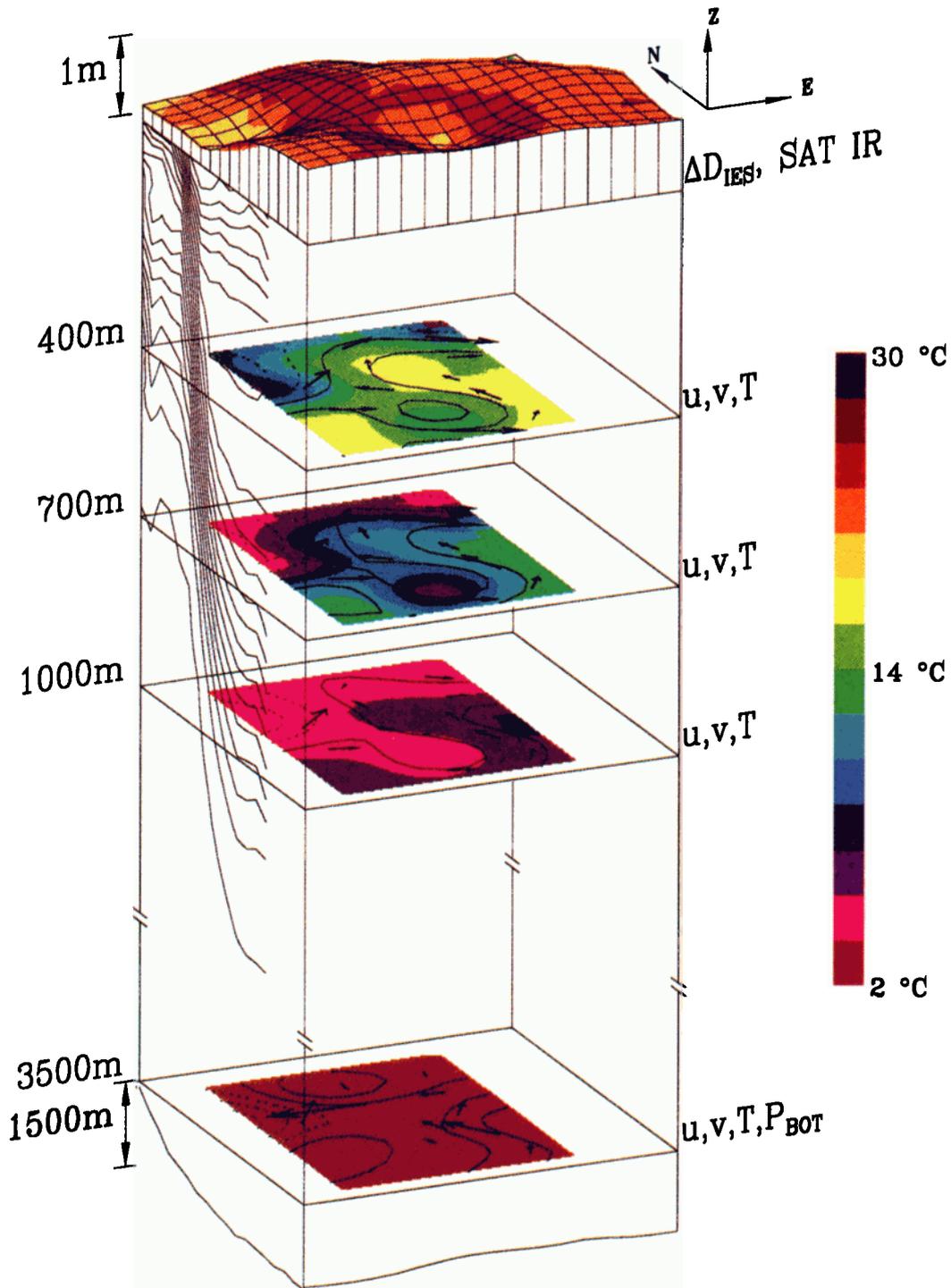
Plate 2. Three-dimensional view of the Gulf Stream in the Central Array on November 13, 1989, constructed from observations. The the dynamic height of the sea surface mapped by the IES array is plotted as the raised mesh of the uppermost level. Superimposed on the mesh are the satellite-derived SSTs of the image shown in Plate 1, with temperatures coded according to the color bar at the right. The streamfunctions ψ mapped by current meters at 400, 700, and 1000 m are contoured at the middle three levels, and the P_{3500} field is contoured at the bottom. At each depth level, the observed current vectors indicate the speed and direction of flow. In order to represent the strongly-sheared velocity structure, both the ψ contour interval and the vector lengths are successively scaled by a factor of 1.5 between levels (e.g., the same vector length at 3500, 1000, 700, or 400 m would indicate speeds of 10, 15, 23, or 34 cm s^{-1}, respectively). Superimposed on the ψ and P_{3500} maps are independently measured (by current meters) temperature fields at each depth; these are coded consistently at all levels using the same color palette. The stream coordinates mean temperature section at 73°W measured by the Pegasus profiler [*Halkin and Rossby*, 1985] is shown on the side panel. The depth scale is linear only from 0 to 1500 m; relative to this the surface dynamic topography is greatly stretched, and the bottom topography is squashed and schematic.

meander that develops by drawing energy from the potential energy of the basic baroclinic state. In fact, this feature did continue to develop and a the ring broke off from the Gulf Stream within 7 days.

Summary

This article, denoted Part 1, and T. J. Shay et al. (submitted manuscript, 1995), denoted Part 2, present a combined overview of the SYNOP Inlet and Central Array experiments. The measurements resolved the baroclinic frontal structure and the currents through the upper and lower water column with synoptic mesoscale resolution for over 2 years.

Whereas near 74°W the variability was typified by small amplitude, near-sinusoidal, propagating and growing meanders, near 68°W steep meanders frequently appeared. Typically, the meander crests propagated through the region, but several troughs stalled and steepened, developed convoluted paths, and formed and interacted with Gulf Stream rings. These steep troughs contributed to the high path displacement variance at all the long periods, especially periods ≥ 85 days.

The region near 69°–70°W has long been known to be a relative "node" in the meander envelope for the Gulf Stream. The lower variance of this node did not result from a uniform decrease across the spectrum, as evidenced by the relatively constant variance in the 25- to 50-day band throughout the region 70°–67°W. Instead the lower nodal variance resulted from greatly decreased spectral variance at periods longer than 85 days. The Kontoyiannis and Watts [1994] and Lee [1994] studies have explained this observation by the existence of long-period (roughly semiannual to annual) standing waves in the Gulf Stream path with half wavelength equal to the distance from Cape Hatteras to 69°–70°W.

Because steep troughs form preferentially near 68°W, even the long-term mean fields display a weak trough there. The mean frontal and current structure show primary and secondary effects associated with this mean trough. While the vertically sheared currents are basically aligned along the curved front in an "equivalent barotropic" sense, the currents approaching or leaving the trough at two sites exhibit, respectively, backing or veering. Thus even in the mean fields there is evidence supporting meander crest/trough associated cross-frontal motion and associated downwelling or upwelling.

Daily time series maps have confirmed earlier inferences that the Gulf Stream is always present and strong in the 68°W region and has remarkably steady cross-stream structure in the upper level front and jet of the current, when viewed in stream coordinates (see further developments by Johns et al. [1995]). However, this study has demonstrated additionally that the cross-stream slope of the thermocline varies with path curvature in accord with the gradient wind balance.

In six representative events, the deep pressure fields vary from essentially featureless to exhibiting remarkably intense cyclones and anticyclones. At times the deep flow is nearly aligned with that of the upper jet, while at other times the flows are approximately normal. The fact that the most intense deep circulations are observed only when the upper jet meandered energetically suggests that the two layers are vertically coupled and jointly evolve. Analyses are in progress to understand this coupling.

Detailed dynamical case studies are also underway and are beyond the scope of this paper; however, two cases of baroclinic instability have been illustrated. In one event (November 25, 1989) the temperature and streamfunction fields in the thermocline were offset about one-sixteenth to one-sixth wavelength.

Emerging from these and other recent studies is a new view of the Gulf Stream. This is achieved because of advancements in both observational and data analysis techniques. The variety of processes that occur is thought provoking. A correct dynamical understanding of the Gulf Stream requires knowledge of the structure of its density and flow fields, and must account for intrinsically associated vertical and cross-frontal motions and the consequent coupling between the deep and shallow layers. With the ability to map the four-dimensional structure of mesoscale events, these associations may be visualized and quantified. Altogether, these data provide rich grounds for further dynamical and modeling studies.

References

Bretherton, F. P., R. E. Davis, and C. B. Fandry, A technique for objective analysis and design of oceanographic experiments applied to MODE-73, *Deep Sea Res., 23,* 559–582, 1976.

Bronshtein, I. N., and K.A. Semendyayev, *Handbook of Mathematics,* edited by K.A. Hirsch, English translation by H. Deutsch, Frankfurt, Germany, distributed by Van Nostrand Reinhold, New York, 1985.

Cornillon, P., The effect of the New England seamounts on Gulf Stream meandering as observed from satellite IR imagery, *J. Phys. Oceanogr., 16,* 386–389, 1986.

Cronin, M., Eddy-mean flow interaction in the Gulf Stream at 68°W, Ph.D. thesis, Univ. of R. I., Narragansett, 1993.

Cronin, M., E. Carter, and D.R. Watts, Prediction of the Gulf Stream path from upstream parameters, *J. Geophys. Res., 97,* 7257-7269, 1992a.

Cronin, M., K. L. Tracey, and D. R. Watts, Mooring motion correction of SYNOP Central Array current meter data,

Tech. Rep. 92–4, Grad. School of Oceanogr., Univ. of R. I., Narragansett, 1992b.

Cushman-Roisin, B. L., L. J. Pratt, and E. Ralph, A general theory of equivalent barotropic thin jet, *J. Phys. Oceanogr., 92,* 749–754, 1993.

Fields, E., and D. R. Watts, The SYNOP experiment: Inverted echo data report for May 1988 to August 1989, *Tech. Rep. 90–2,* Grad. School of Oceanogr., Univ. of R. I., Narragansett, 1990.

Fields, E., and D. R. Watts, The SYNOP experiment: Inverted echo sounder data report for June 1989 to September 1990, *Tech. Rep. 91–2,* Grad. School of Oceanogr., Univ. of R. I., Narragansett, 1991.

Fofonoff, N. P., The Gulf Stream system, in *Evolution of Physical Oceanography,* edited by B. A. Warren and C. Wunsch, pp. 112–139, MIT Press, Cambridge, Mass., 1981.

Gilman, C. S., A study of the Gulf Stream downstream of Cape Hatteras 1975–1986, M. S. thesis, Univ. of R. I., Narragansett, 1988.

Halkin, D., and H. T. Rossby, The structure and transport of the Gulf Stream at 73°W, *J. Phys. Oceanogr., 15,* 1439–1452, 1985.

Hall, M. M., and H. L. Bryden, Profiling the Gulf Stream with a current meter mooring, *Geophys. Res. Lett., 12,* 203–206, 1985.

Halliwell, G. R., and C. N. K. Mooers, Meanders of the Gulf Stream downstream from Cape Hatteras 1975–1978, *J. Phys. Oceanogr., 13,* 1275–1292, 1983.

Hansen, D. V., and G. A. Maul, A note on the use of sea surface temperature for observing ocean currents, *Remote Sens. Environ., 1,* 161–164, 1970.

He, Y., Determining the baroclinic geostrophic velocity structure with inverted echo sounders, M. S. thesis, Univ. of R. I., Narragansett, 1993.

Hogg, N. G., Toward parameterization of the eddy field near the Gulf Stream, *Deep Sea Res., Part A, 40,* 2359–2376, 1993.

Holton, J. R., *An Introduction to Dynamic Meteorology,* Academic, San Diego, Calif., 1979.

Horton, C. W., Modulation of Gulf Stream surface-subsurface frontal separation by path curvature, *J. Phys. Oceanogr., 17,* 596–603, 1987.

Howden, S. D., E. Fields, X. Qian, K. Tracey, and D. R. Watts, IES calibration for main thermocline depth: A method using integrated XBT temperature profiles, *Tech. Rep. 93–3,* Grad. School of Oceanogr., Univ. of R. I., Narragansett, 1993.

Johns, W. E., and R. J. Zantopp, The SYNOP experiment: Moored acoustic doppler current profiler data for the period June 1988 to August 1990, *Tech. Rep. 91–003,* Rosenstiel School Mar. Atmos. Sci., Univ. of Miami, Miami, Fla., 1991.

Johns, W. E., T. J. Shay, D. R. Watts, and J. M. Bane, Gulf Stream structure, transport and recirculation at 68°W, *J. Geophys. Res., 100,* 817–838, 1995.

Kelly, K. A., The meandering Gulf Stream as seen by Geosat altimeter: Surface transport, position, and velocity variance from 73° to 46°W, *J. Geophys. Res., 96,* 16,721–16,738, 1991.

Kelly, K. A., and D. R. Watts, Monitoring Gulf Stream transport by radar altimeter and inverted echo sounders, *J. Phys. Oceanogr., 24,* 1080–1084, 1994.

Kim, H.-S., An equivalent-barotropic data-assimilating model of Gulf Stream meanders, Ph. D. thesis, Univ. of R. I., Narragansett, 1994.

Kim, H.-S., and D. R. Watts, An observational streamfunction in the Gulf Stream, *J. Phys. Oceanogr, 24,* 2639–2657, 1994.

Kontoyiannis, H., and D. R. Watts, Observations on the variability of the Gulf Stream path between 74°W and 70°W, *J. Phys. Oceanogr., 24,* 1999–2013, 1994.

Lee, T., Variability of the Gulf Stream path observed from satellite infrared images, Ph. D. thesis, Univ. of R. I., Narragansett, 1994.

Little, J. N., and L. Shure, *Signal Processing Toolbox for use with MATLAB,* MathWorks, Inc., Natick, Mass., 1993.

Luyten, J. R., Scales of motion in the deep Gulf Stream and across the continental rise, *J. Mar. Res., 35,* 49–74, 1977.

Manning, J. P., and D. R. Watts, Temperature and velocity structure of the Gulf Stream northeast of Cape Hatteras: Principal modes of variability, *J. Geophys. Res., 94,* 4879–4890, 1989.

Palmén, E., and C. W. Newton, *Atmospheric circulations systems,* Acadmic, San Diego, Calif., 1969.

Pickart, R. S., Interaction of the Gulf Stream and deep western boundary current where they cross, *J. Geophys. Res., 99,* 25,155–25,164, 1994.

Pickart, R. S., Gulf Stream–generated topographic Rossby waves, *J. Phys. Oceanogr., 25,* 574–586, 1995.

Pickart, R. S., and D. R. Watts, Using the inverted echo sounder to measure vertical profiles of Gulf Stream temperature and geostrophic velocity, *J. Atmos. Oceanic Technol., 7,* 146–156, 1990.

Pickart, R.S., X. Qian, and D.R. Watts, The SYNOP inlet experiment: Bottom current meters for October 1987 to August 1990 mooring period, *Tech. Rep. 91–1,* Grad. School of Oceanogr., Univ. of R. I., Narragansett, 1991.

Qian, X., and D. R. Watts, The SYNOP experiment: Bottom pressure maps for the Central Array May 1988 to August 1990, *Tech. Rep. 92–3,* Grad. School of Oceanogr., Univ. of R. I., Narragansett, 1992.

Qian, X., K. Tracey, E. Fields, and D. R. Watts, The SYNOP experiment: Inverted echo sounder data report for October 1987 to 1988, *Tech. Rep. 90–3,* Grad. School of Oceanogr., Univ. of R. I., Narragansett, 1990.

Richardson, P. L., Gulf Stream rings, in *Eddies in Marine Science,* edited by A. Robinson, pp. 19–45, Springer-Verlag, New York, 1983.

Robinson, A. R., M. A. Spall, and N. Pinardi, Gulf Stream simulations and the dynamics of ring and meander processes, *J. Phys. Oceanogr., 18,* 1811–1853, 1988.

Savidge, D. K., and J. M. Bane, Observation of predicted deep cyclone at 68°W, 37°N, *EOS Trans. AGU, 75,* (3), Ocean Sci. Meet. Suppl., 148, 1994.

Schmitz, W. J., A. R. Robinson, and F. C. Fuglister, Bottom velocity observations directly under the Gulf Stream, *Science, 170,* 1192–1194, 1970.

Shay, T. J., S. Haines, J. M. Bane, and D. R. Watts, SYNOP Central Array current meter data report: Mooring period May 1988-September 1990. *Tech. Rep. CMS 91–2,* 106 pp. Univ. of N. C., Chapel Hill, 1994.

Tracey, K. L., and D. R. Watts, On Gulf Stream meander characteristics near Cape Hatteras, *J. Geophys. Res., 91,* 7587–7602, 1986.

Tracey, K. L., and D. R. Watts, The SYNOP experiment: Thermocline depth maps for the Central Array for October 1987 to August 1990, *Tech. Rep. 91–5,* Grad. School of Oceanogr., Univ. of R. I., Narragansett, 1991a.

Tracey, K. L., and D. R. Watts. The SYNOP experiment: Thermocline depth maps for the Inlet Array October 1987 to August 1990. *Tech. Rep. 91–6,* Grad. School of Oceanogr., Univ. of R. I., Narragansett, 1991b.

Watts, D. R., Gulf Stream variability, in *Eddies in Marine Science,* edited by A. Robinson, pp. 114–144, Springer-Verlag, New York, 1983.

Watts, D. R., Equatorward currents in temperatures 1.8–6.0°C on the Continental Slope in the Mid-Atlantic Bight, in *Deep Convection and Deep Water Formation in the Oceans*, edited by G. C. Gascard and P. C. Chu, Elsevier Oceanography Series, v. 51, Elsevier, New York, 1991.

J. M. Bane and T. J. Shay, Marine Sciences Program, University of North Carolina, Chapel Hill, NC 27599. (e-mail: bane@marine.unc.edu; shay@marine.unc.edu)

K. L. Tracey and D. R. Watts, University of Rhode Island, Graduate School of Oceanography, Narragansett Bay Campus, Narragansett, RI 02882-1197. (e-mail: karen@calvin.gso.uri.edu; randy@drw.gso.uri.edu)